Provenance of synorogenic deposits of the Upper Cretaceous–Lower Palaeogene Jarmuta–Proč Formation (Pieniny Klippen Belt, Western Carpathians)

JOZEF MADZIN[1,✉], DUŠAN PLAŠIENKA[2] and ŠTEFAN MÉRES[3]

[1]Earth Science Institute, Slovak Academy of Sciences, Ďumbierska 1, 974 01 Banská Bystrica, Slovakia; ✉jozef.madzin@savba.sk
[2]Department of Geology and Palaeontology, Faculty of Natural Sciences, Comenius University, Mlynská dolina, Ilkovičova 6, 842 15 Bratislava, Slovakia; dusan.plasienka@uniba.sk
[3]Department of Geochemistry, Faculty of Natural Sciences, Comenius University, Mlynská dolina, Ilkovičova 6, 842 15 Bratislava, Slovakia; stefan.meres@uniba.sk

(Manuscript received July 12, 2018; accepted in revised form January 11, 2019)

Abstract: The Pieniny Klippen Belt contains thickening and coarsening upwards synorogenic sedimentary successions witnessing the collision of the Oravic ribbon continent with the Central Carpathian orogenic wedge after the closure of the Vahic Ocean in the Late Cretaceous to Early Palaeogene. The sedimentary record of this event is represented by flysch/wildflysch deposits of the Maastrichtian–Lower/Middle Eocene Jarmuta–Proč Formation. We present results of the provenance study of these deposits, based on the framework petrography, heavy mineral analysis and mineral chemistry. Turbiditic sandstones were classified as quarzolithic to lithic arenites. Lithic fragments are predominantly composed of carbonate rocks and low- to medium-grade metamorphic and occasional mafic volcanic rocks. The heavy mineral association is composed of both first-cycle derived and recycled ultrastable ZTR, garnets and Cr-spinels. The chemistry of the detrital tourmalines and garnets suggests a derivation from various low- to medium-grade metamorphic rocks. High-pyrope garnets, observed in the eastern part of the PKB, which were derived from high-grade granulites and eclogites, represent probably lower crustal complexes exhumed during rifting of the Vahic Ocean. The Cr-spinels show a mixed harzburgitic and lherzolitic provenance. The harzburgitic Cr-spinels might have been recycled from older exotic conglomerates of the Klape Flysch, thereby representing ophiolitic detritus of the Meliata Ocean. The lherzolitic Cr-spinels might represent a new contribution of ophiolitic detritus delivered from the exhumed subcontinental mantle forming the Vahic oceanic floor.

Keywords: Western Carpathians, Pieniny Klippen Belt, synorogenic deposits, petrography, heavy mineral analysis, mineral chemistry, provenance.

Introduction

The Pieniny Klippen Belt (PKB) is one of the structurally most complicated zone of the Western Carpathians (WC), separating the External Western Carpathians (EWC; Tertiary accretionary complex — Flysch Belt) from the Central Western Carpathians (CWC; Cretaceous Austroalpine–Slovako-carpathian basement–cover thrust stack) (e.g., Plašienka et al. 1997; Plašienka 1999, 2018a; Froitzheim et al. 2008).

The PKB includes Jurassic to Palaeogene sediments detached from its completely subducted basement of unknown character. Its complex polyphase structural deformation dominated by the Palaeocene to Eocene nappe thrusting resulted in the superposition and juxtaposition of numerous lithologically and palaeogeographically distinct tectonic units (see e.g., Birkenmajer 1977, 1986; Mišík 1997; Jurewicz 2005; Plašienka & Mikuš 2010; Plašienka 2012a). Later, during the Early and Middle Miocene, the PKB experienced further strong deformation including out-of-sequence thrusting, transpression, transtension, backthrusting, and block rotations, which obliterated original fold-and-thrust structures resulting in its complicated spectacular "klippen" structure (e.g., Ratschbacher et al. 1993; Kováč & Hók 1996; Plašienka & Jurewicz 2006; Plašienka 2012b, 2018b). Therefore, the PKB is often characterized as a peculiar block-in-matrix structure or mélange formed by isolated rigid blocks "klippen" composed of competent Middle Jurassic to Lower Cretaceous carbonates surrounded by a soft matrix of the "klippen mantle" consisting of Lower Jurassic and Upper Cretaceous to Palaeogene shales, marls and flysch formations (e.g., Birkenmajer 1977; Plašienka & Mikuš 2010).

The main tectonic units of the PKB s.s., were derived from an independent palaeogeographic domain known as the Oravic domain or Oravicum (Maheľ 1986). It is thought that the Oravic domain represents the continental crustal fragment in the Middle Penninic position (analogous to the Briançonnais microcontinent) surrounded by North Penninic (Valais–Rhenodanubian–Magura) (e.g., Schmid et al. 2008) and South Penninic (Ligurian–Piemont–Vahic–Iňačovce) oceanic domains as a continuation of the Alpine Atlantic oceanic tract from the Alps to the Carpathians (Plašienka 2003, 2012a; Froitzheim et al. 2008; Plašienka & Soták 2015). Consequently, the supposed suture-like structure of the PKB, although ophiolites do not participate in its recent surface structure, is related to the collision of the Oravic ribbon continent with the frontal parts of the CWC orogenic wedge after the closure and subduction of the Vahic oceanic domain (Plašienka 2012a). Whether, and to what extent, the Vahic (South Penninic) and likewise the Magura (North Penninic) basins, were floored by an oceanic crust is still a matter of debates and controversy (e.g., Winkler & Ślączka 1992, 1994; Rakús & Hók 2005; Aubrecht et al. 2009; Oszczypko et al. 2015).

The sedimentary record of the contractional tectonic processes is represented by a turbiditic sequence of the Turonian Snežnica Fm. and the Coniacian–Santonian Sromowce Fm. including bodies of exotic conglomerates (Pieniny Unit; Plašienka 2012a and references therein), and the Upper Cretaceous–Lower/Middle Eocene synorogenic flysch or wildflysch Jarmuta–Proč Formation consisting of turbiditic sandstones with huge olistostromatic bodies (Gregorianka Breccia Member of the Sub-Pieniny Unit and Milpoš Breccia Member of the Šariš Unit) (Plašienka & Mikuš 2010; Plašienka 2012a; Plašienka et al. 2012).

Rocks referable to the Jarmuta Fm. or to the Jarmuta–Proč Fm. have been known since the 1930s (e.g., Horwitz 1932). However, data about its sedimentology, petrography (Leško 1960; Ďurkovič 1972), heavy mineral composition (Starobová 1962; Łoziński 1966; Winkler & Ślączka 1992, 1994), and mineral chemistry (Salata 2002, 2004; Oszczypko & Salata 2005; Bónová et al. 2018) are contradictory in some aspects (e.g., Birkenmajer 1977, 1986; Nemčok et al. 1989; Plašienka & Mikuš 2010). On the other hand, the cited works suggest the crucial importance of the synorogenic sediments for understanding the early development of the PKB (Plašienka & Mikuš 2010; Plašienka et al. 2012).

The aim of this paper is to contribute to the provenance analysis of the Jarmuta–Proč Fm. based on the framework petrography, heavy mineral analysis and mineral chemistry of detrital tourmalines, garnets and Cr-spinels.

Geological settings

Most of the samples were collected from the Pieniny, Šariš and Beňatina sectors (according to the classical division by Scheibner 1967; Vass 1988; Mišík 1997) of the PKP in eastern Slovakia (Fig. 1). Recently, a new model for the structure and development of the PKB has been demonstrated from this area (Plašienka & Mikuš 2010; Plašienka 2012b; Plašienka et al. 2012). Three principal superposed Oravic tectonic units of the PKB have been distinguished. These are the Šariš (formerly named Fakľovka Unit by Plašienka & Mikuš 2010), the Sub-Pieniny and Pieniny thrust sheets from bottom to top. All of the Oravic units are characterized by varied Jurassic to Upper Cretaceous–Palaeogene coarsening- and thickening-upwards synorogenic sedimentary successions deposited in the front of the advancing thrust sheets (Fig. 2).

The Šariš unit (for more details see Plašienka & Mikuš 2010; Plašienka 2012a,b; Plašienka et al. 2012) occurs in the lowermost structural position and includes a strongly dismembered basinal Jurassic to Lower/Middle Eocene sedimentary succession. The top of the Šariš unit is composed of a hundred metres of sandstone-dominated flysch or wildflysch sequence of the latest Cretaceous to Lower/Middle Eocene Jarmuta–Proč Fm. (JPF) with bodies of mass-transport deposits including numerous huge olistoliths (Milpoš Breccia Member; Plašienka & Mikuš 2010). A variegated clastic material and olistoliths were mainly derived from sedimentary successions of the overriding Sub-Pieniny and Pieniny nappes (Plašienka & Mikuš 2010).

The Sub-Pieniny Unit exhibits an intricate structure including the typical shallow-marine Middle Jurassic to Lower Cretaceous Czorsztyn succession, as well as the slope-derived "transitional" Niedzica/Czertezik successions (e.g., Ožvoldová et al. 2000; Wierzbowski et al. 2004). The sedimentary succession of the Sub-Pieniny Unit is terminated by comparatively thin calcareous sandstones of the JPF (Maastrichtian–Danian?), which includes mass-transport deposits in the upper parts (Gregorianka Breccia Member; Nemčok et al. 1989; redefined by Plašienka & Mikuš 2010). The Gregorianka Breccia Member is composed of monotonous detrital material derived evidently from the overriding Pieniny nappe (Plašienka et al. 2012).

The Pieniny Unit occurs in the most internal and the uppermost structural position of the PKB tectonic entity as a laterally continuous thrust sheet (Plašienka 2012b). It comprises mainly a deep-water Jurassic to Upper Cretaceous succession terminated by a coarsening- and thickening-upwards synorogenic turbiditic sequence of the Turonian Snežnica Fm. and the Coniacian–Santonian Sromowce Fm. (Plašienka 2012a).

Methods

Framework petrography

The framework petrography was carried out on 72 sandstone samples of the JPF taken from 15 geographically distributed localities throughout the PKB (Fig. 1, Supplementary Table S1). Petrographic features of the sandstones including mineral constituents, grain size, sorting, and roundness were observed by using a polarizing microscope. The samples were selected from medium to coarse-grained sandstones in order to get the maximum source rock information. In order to eliminate different grain size issues (Ingersoll et al. 1984), analyses from the individual grain-sizes were plotted separately in the classification diagrams (Figs. 3, 4). At least 300 grains in each thin section were counted. The point-counting method followed the approach of von Eynatten & Gaupp (1999). This approach is more useful in synorogenic coarse-grained sediments than the classical Gazzi–Dickinson method (the GD method as described by Ingersoll et al. 1984), where minerals or crystals >63 μm in polycrystalline fragments are counted separately. For example, following the GD method, a significant amount of polycrystalline mica–quartz aggregates would

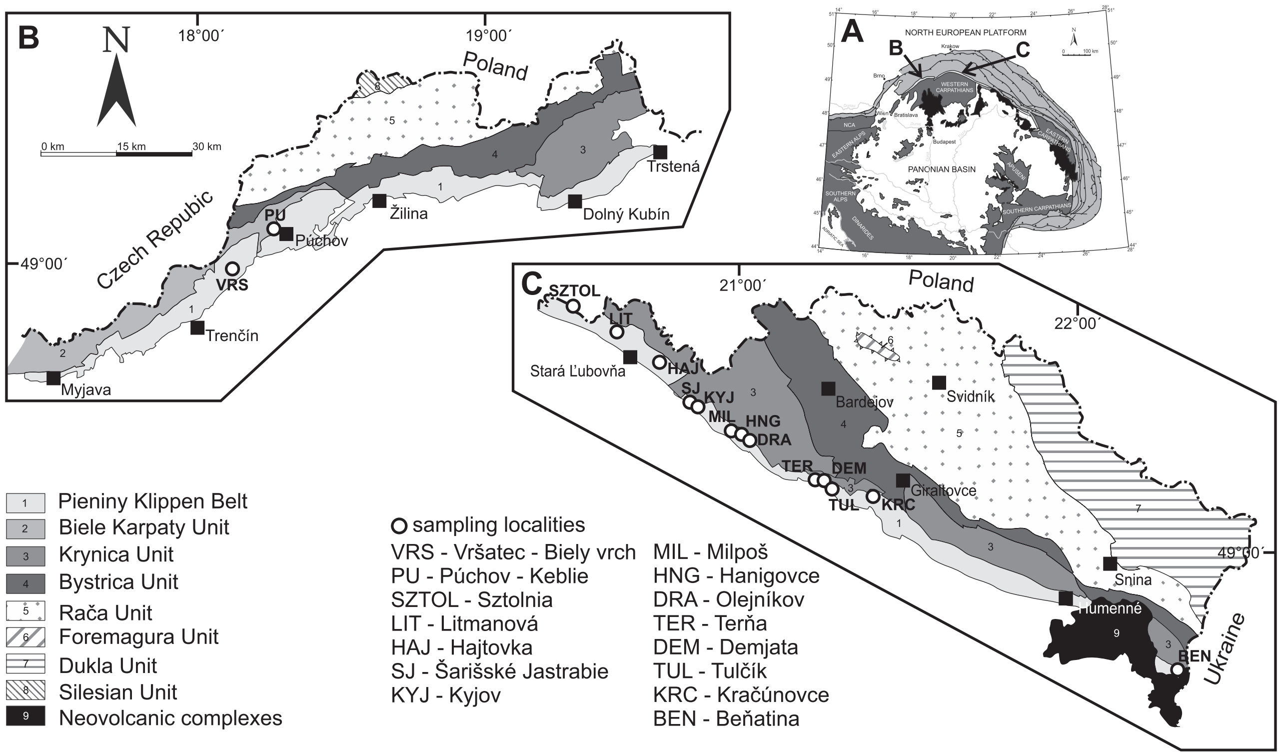

Fig. 1. A — Location of the study areas in the frame of the Alpine–Carpathian–Pannonian–Dinaridic tectonic system; **B, C** — tectonic sketch maps with location of the sampled sites (modified after Kováč et al. 1998; Bezák et al. 2004).

be assigned to the monocrystalline quartz category, thereby a metamorphic origin of these clasts may be overlooked. Because of the high amount of carbonate clasts (L_{carb}= limestones+dolomites), they were attributed to the category of lithic fragments (L) together with other non-carbonate lithic fragments (L_s), which is not usual in classic provenance studies (Dickinson & Suczek 1979; Dickinson 1985). However, carbonate clasts were eroded and transported through the same processes as any clastic material and overlooking and non-counting of the carbonate clasts would have led to a partly incorrect classification of the analysed rocks, and therefore, to a biased provenance interpretation. Carbonate allochems, such as intrabasinal carbonate bioclasts, following discrimination criteria proposed by Zuffa (1985) were not counted.

Heavy mineral analysis

Ten samples of medium- to coarse-grained sandstones/fine-grained conglomerates of the JPF and Milpoš Breccia Mb. (MB) were selected for the heavy mineral analysis (Table 1). The separation and preparation of heavy minerals followed the standard procedures described by Mange & Mauer (1992). The 80–250 μm fraction was examined under both a polarizing and a binocular microscope. At least 200 grains were counted using the ribbon counting method (Galehouse 1971) and are shown as number percentages (Table 2).

Mineral chemistry

Detrital tourmalines, garnets and Cr-spinels from the selected sandstone samples (Table 1) were hand-picked, mounted in epoxy resin, polished and coated with carbon for electron microprobe analysis.

The chemical composition of the separated detrital minerals were analysed using a CAMECA SX-100 electron microprobe at State Geological Institute of Dionýz Štúr in Bratislava. The analytical conditions were a 15 kV accelerating voltage and a 20 nA beam current with peak counting time of 20 s and a beam diameter of 2–10 μm. Raw counts were corrected using a PAP matrix correction (Pouchou & Pichoir 1985).

To measure various elements the following natural and synthetic standards were used: wollastonite ($SiK_α$, $CaK_α$), TiO_2 ($TiK_α$), Al_2O_3 ($AlK_α$), pure Cr ($CrK_α$), pure V ($VK_α$), fayalite ($FeK_α$), rhodonite ($MnK_α$), forsterite ($MgK_α$), willemite ($ZnK_α$), pure Ni ($NiK_α$), albite ($NaK_α$), orthoclase ($KK_α$), BaF2 ($FK_α$) and NaCl ($ClK_α$). Lower detection limits of the measured elements varied between 0.01 and 0.05 wt. %; V, Cr, Mn, Zn, Ni, F, and Cl were also below their respective detection limits.

Overall 45 analyses of detrital tourmalines from five JPF and two MB samples were performed (Suppl. Table S2). Detrital tourmalines were analysed by using one to three single-spots located over centres and/or along rims of grains. The crystallo-chemical formulae of tourmaline were calculated on the basis of 15 Y+Z+T cations, $^{W}O^{2-}$ was obtained from the charge-balanced formula, OH was calculated as OH=4−Cl−^{W}O apfu, B=3 apfu.

Overall 35 analyses of detrital garnets separated from seven localities of the JPF and MB were performed (Suppl. Table S3). The crystallo-chemical formula of garnet was normalized to 12 oxygens and conversion of iron valence (Fe^{3+} and Fe^{2+}) according to ideal stoichiometry.

Chemical compositions of 15 detrital Cr-spinels from six localities of the JPF and MB were examined (Suppl. Table S4). Analyses of detrital Cr-spinels were calculated on the basis of 3 cations. Fe^{2+} and Fe^{3+} in spinel were allocated according to the ideal stoichiometry.

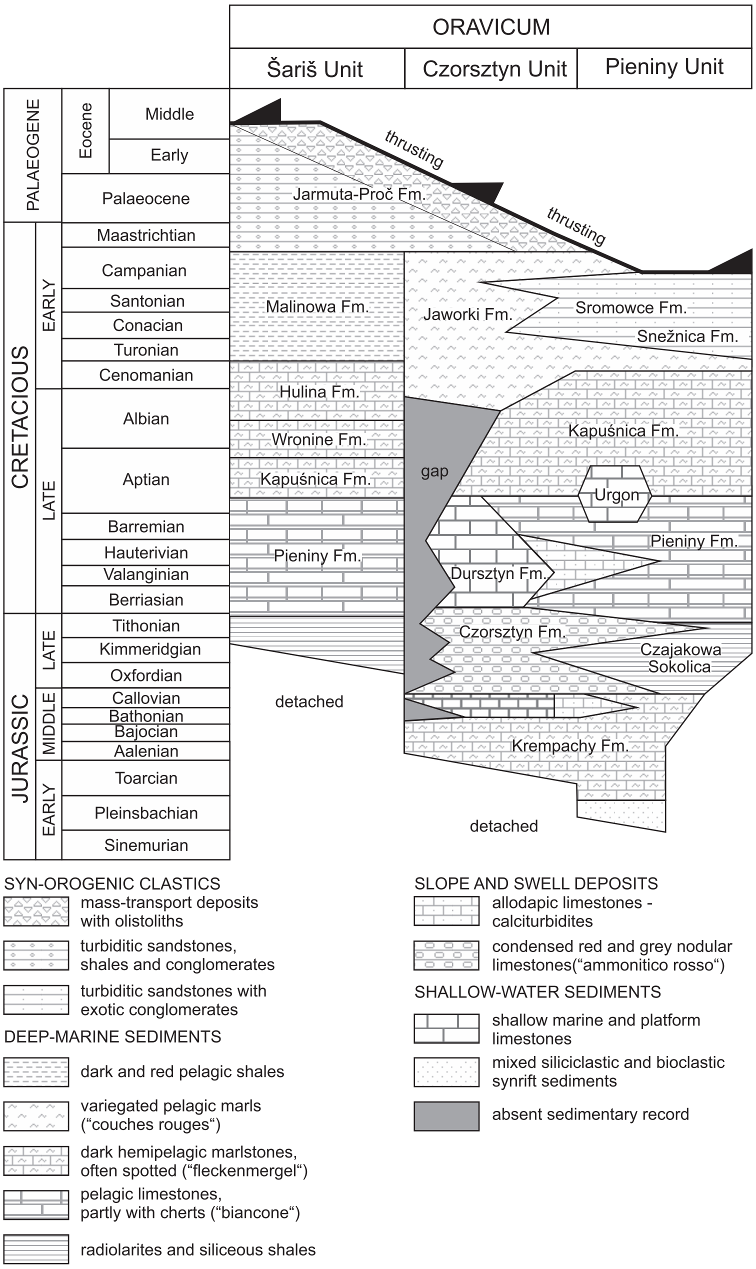

Fig. 2. Lithostratigraphic column of the Oravic tectonic units of the PKB (after Plašienka 2012a).

Results

Framework petrography

The JPF consist mainly of grey, grey brown, and grey blue fine- to coarse- and very coarse-grained sandstones/fine-grained conglomerates with occasional intercalations of calcareous grey to grey brown mudstones. It is apparent that the detrital material of the sandstones and their coarse-grained equivalents, the Milpoš Breccia Member, is the same.

Texturally, the studied sandstones can be regarded as sub-mature, since they are moderately sorted, composed mostly of angular, sub-angular to sub-rounded grains (Fig. 5). Compositionally, the sandstones are immature, because of the high content of lithic, mostly carbonate grains. The matrix of the sandstones occurs very rarely and the sandstones are cemented mostly by carbonate cement. According to the classification scheme introduced by Pettijohn et al. (1972), the analysed sandstones are predominantly lithic arenites, less sub-lithic arenites and one sample is characterized as sub-arcosic arenite (Fig. 3A). Based on the classification diagram proposed by Garzanti (2016) the studied sandstones are classified predominantly as litho–quartzitic, feldspatho–litho–quartzitic to quartzo–lithic sandstones and one sample as feldspatho–quartzitic sandstone (Fig. 3B). Medium-grained sandstones plot in the classification diagrams closer to the Q pole than their coarse-grained equivalents.

The main components of the sandstones are quartz (Q) and lithic grains (L).

Quartz (Q_t) is represented by both monocrystalline and polycrystalline forms. The monocrystalline quartz (Q_m) is a ubiquitous component of the analysed sandstones. The polycrystalline quartz (Q_p) consists of either a fine-grained chert and/or a mica-quartz aggregate mostly of a metamorphic origin.

Feldspar contents (F) are usually low (on average about 3 %) (Figs. 3, 4; Suppl. Table S1). K-feldspars outweigh plagioclases and are represented by orthoclase, with occasional perthitic texture. All feldspars are strongly altered.

Lithic grains constitute on average about 40 % of the total framework grains (Suppl. Table S1). They are represented by metamorphic grains (L_{met}), volcanic grains (L_v), grains of siliciclastic sedimentary rocks (L_p), and grains of carbonate rocks (L_{carb}). Grains of carbonate rocks include mostly limestones, marly limestones, marls (L_{lim}), and dolomites (D).

The most common type of metamorphic grains (Fig. 5B–E) are mica–quartz aggregates derived from low- to medium-grade metamorphic rocks

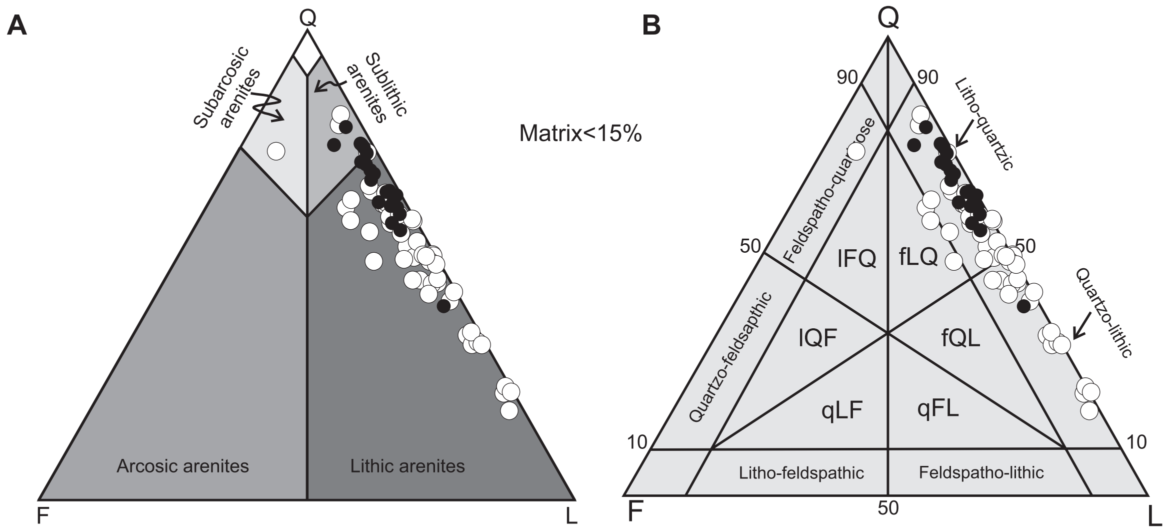

Fig. 3. Classification of the sandstones studied based on their grain composition: **A** — Pettijohn et al. (1972); **B** — Garzanti (2016). Black dots — medium-grained sandstones; white circles — coarse-grained sandstones. Q — quartz, F — feldspar, L — lithic fragments including lithoclasts of carbonates.

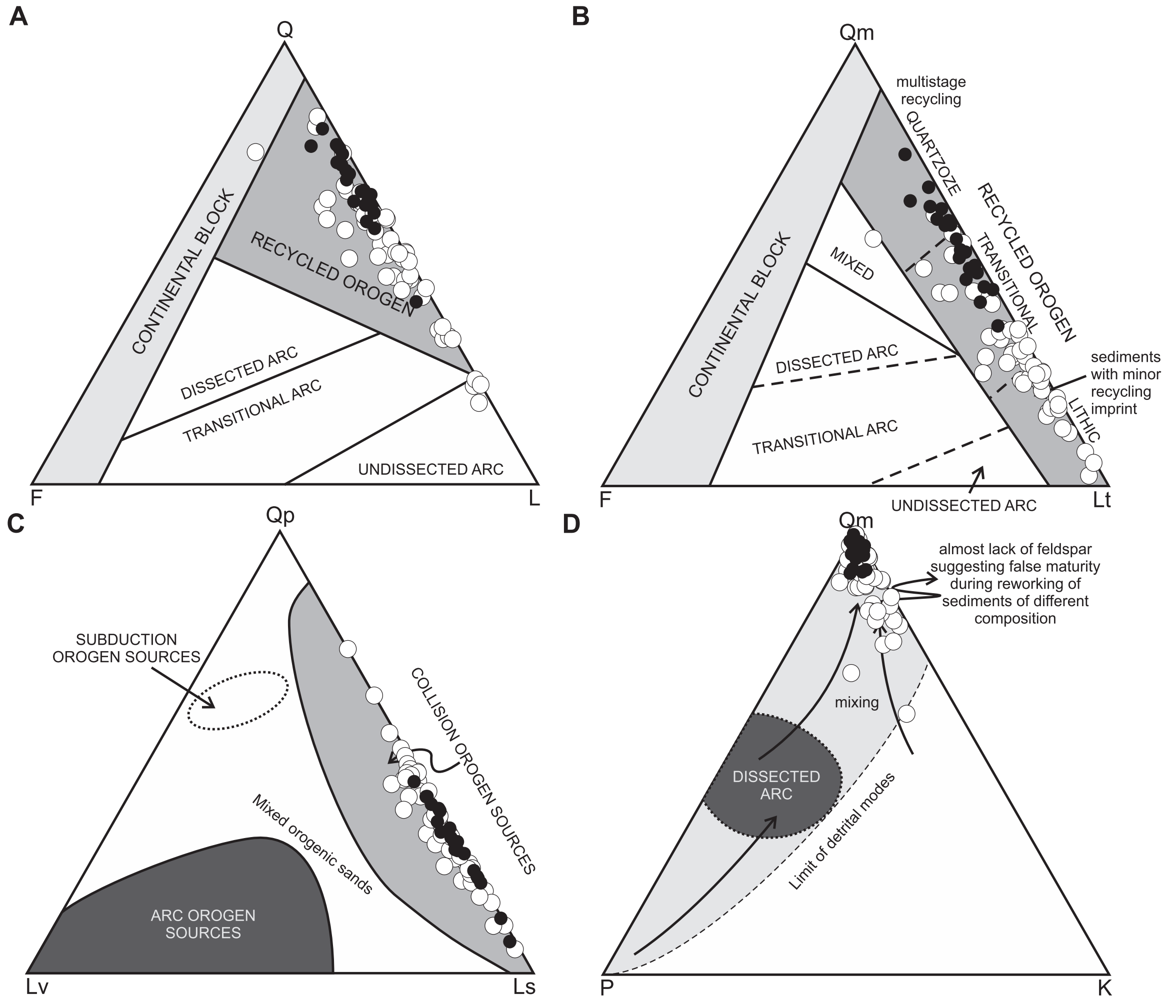

Fig. 4. Ternary provenance discrimination diagrams for the sandstones studied (fields after Dickinson & Suczek 1979; Dickinson 1985). Black dots — medium-grained sandstones; white circles — coarse-grained sandstones. Q — quartz, Q_m — monocrystalline quartz, Q_p — polycrystalline quartz, F — feldspar, K — K-feldspar, L — lithoclasts including lithoclasts of carbonates, L_s — sedimentary clasts, L_t — total lithics including carbonate lithoclasts, L_v — volcanic clasts.

(following discrimination criteria by Garzanti & Vezzoli 2003). Grains of low-grade metamorphic siliciclastic sedimentary rocks (Fig. 5B–C) and grains of metabasic rocks also occur. The amounts of metamorphic grains vary in the range of 0.0–26 %, (on average ~9 %) (Suppl. Table S1).

Grains of volcanic rocks occur in the subordinate amount of 1 % (Suppl. Table S1) and are represented mostly by basic volcanic rocks (Fig. 5F).

Grains of siliciclastic sedimentary rocks constitute about 1 % of the whole-rock composition. Grains of carbonates of the klippen succession provenance (Fig. 5B) are the most frequent lithoclasts in the JPF, and their content varies in the range from 0 to 64 % (on average of 21 %) (Suppl. Table S1).

Heavy mineral analysis

Almost all examined samples are characterized by a depleted ultrastable association of heavy minerals (ZTR=zircon+tourmaline+rutile). The heavy mineral associations are composed either of prevailing ultrastable ZTR minerals over garnets and apatites (zircon/tourmaline+garnet+apatite) or prevailing garnets over ultrastable ZTR (garnet+zircon/tourmaline+apatite). The Milpoš Breccia Mb. is characterized by the ultrastable ZTR heavy mineral association (Table 2). Almost all the studied samples contain detrital Cr-spinel (up to 13 %). Accessories include epidote, sphene and minerals of the kyanite–sillimanite–andalusite group.

Zircon (Fig. 6A–E) occurs mainly as colourless, yellow or pink grains, with abundant inclusions and zonation. Zircon is represented by subhedral or euhedral grains or their broken fragments. Subrounded to rounded grains are present in subordinate amount. Short stubby grains with crystal elongation (length-to-width ratio) ~2–2.5:1 are most frequent (Fig. 6A). Long prismatic and needle-shape grains (length-to-width ratio >4:1) occur as well.

Tourmaline grains (Figs. 6F–I, 7A–H) are present mostly as euhedral and angular broken fragments prevailing over subrounded to rounded grains. The euhedral varieties very often contain inclusions of zircon. Angular and subrounded grains show initial to advanced stages of corrosion, mainly around rims of grains (Andò et al. 2012) (Fig. 6H). Well rounded grains occur only sporadically. Bright to dark brown to olive green coloured grains predominate. Dark green or blue varieties are less frequent. Salmon pink, colourless or zonal varieties are rare.

Rutiles occur as small mostly subrounded grains and subhedral or prismatic fragments (Fig. 6K–L). Yellow, red and

Table 1: List of sampled sites for heavy mineral analysis, with their geographic coordinates, lithostratigraphy and macroscopic description.

Locality	Sample	GPS		Litostratigraphy	Macroscopic features
		N	E		
Litmanová	LIT-1	49° 22.547’	20° 37.228’	Milpoš Breccia Mb. Šariš Unit	medium/coarse-grained sandstone matrix of coarse-grained carbonate breccia
Hajtovka	H-1B	49° 17.833’	20° 47.002’	Milpoš Breccia Mb. Šariš Unit	medium/coarse-grained sandstone matrix of coarse-grained carbonate breccia
Kyjov	KYJ-1	49° 13.115’	20° 57.861’	Milpoš Breccia Mb. Šariš Unit	medium/coarse-grained sandstone matrix of coarse-grained carbonate breccia
Milpoš	MIL-2	49° 11.824’	21° 00.204’	Milpoš Breccia Mb. Šariš Unit	medium/coarse-grained sandstone matrix of coarse-grained carbonate breccia
Púchov	PU-5	49° 06.125’	18° 16.798’	Jarmuta–Proč Fm. Šariš Unit (Javorina Beds Biele Karpaty Unit sensu Potfaj, 1993)	medium-grained sandstone
Sztolnia	SZTOL-1	49° 24.021’	20° 31.489’	Jarmuta–Proč Fm Šariš (Grajcarek) Unit	coarse-grained sanstone/fine-grained conglomerate
Hajtovka	H-15	49° 18.101’	20° 45.192’	Jarmuta–Proč Fm Šariš Unit	coarse-grained sanstone/fine-grained conglomerate
Olejníkov	DRA-B3	49° 11.543’	21° 03.033’	Jarmuta–Proč Fm Šariš Unit	medium-grained sandstone
Kračúnovce	KRC-5	49° 04.768’	21° 28.276’	Jarmuta–Proč Fm Šariš Unit	medium/coarse-grained sandstone matrix of coarse-grained carbonate breccia
Beňatina	BEN-5	48° 48.922’	22° 20.799’	Jarmuta–Proč Fm Šariš Unit	medium/coarse-grained sandstone matrix of coarse-grained carbonate breccia

Table 2: Frequencies of individual heavy minerals in the sediments studied. Abbreviations of minerals (Whitney & Evans 2010): Zrn — zircon, Tur — tourmaline, Rt — rutile, Grt — garnet, Ap — apatite, Spl — spinel, Ep — epidote, Ttn — titanite (sphene), Ky — kyanite, Sil — sillimanite, And — andalusite.

Sample	Heavy mineral content [%]									
	Zrn	Tu	Rt	Grt	Ap	Sp	Ep	Ttn	Ky–Sil–And	ZTR
LIT-1	16	14	2	34	24	3	7	0	0.0	32
H-1B	24	13	10	24	16	12	0	0	0.9	48
KYJ-1	43	14	16	14	8	3	1	0	0.0	73
MIL-2	17	19	8	29	21	3	0	2	0.0	45
PU-5	28	8	9	47	7	1	0	0	0.0	45
SZTOL-1	27	6	7	50	6	6	0	0	0.0	39
H-15	14	16	6	25	33	4	0	3	0.0	36
DRAB-3	40	11	18	20	3	8	0	0	0.0	69
KRČ-5	28	6	11	46	4	4	1	0	0.0	45
BEN-5	4	8	5	70	8	1	2	0	0.4	18

orange varieties are very frequent. Some rutiles show initial features of corrosion (Andò et al. 2012).

Garnet is represented by angular to subrounded fragments (Figs. 6M–O, 7I–L). Well-rounded grains are very rare. Colourless or salmon pink varieties dominate. Corrosion features point to initial to advanced stages of weathering or intrastratal dissolution (Andò et al. 2012).

Apatite is preserved either as colourless stubby euhedral crystals (Fig. 6P) or as subrounded to rounded grains. Apatites often show initial features of corrosion (Andò et al. 2012).

Spinel occurs mostly as reddish brown angular, subangular to subrounded irregular fragments with characteristic conchoidal breakage patterns (Fig. 6R–S).

Mineral chemistry

Chemistry of detrital tourmalines

The microprobe analysis reveals homogeneous chemistry of the detrital tourmalines. The dominant cation occupying the X-site is Na with a content in the range of 0.44–0.94 *apfu*. Contents of Ca usually display values lower than 0.2 *apfu*. The content of K is very low, not exceeding 0.1 *apfu* (Suppl. Table S2). The X-site vacancy values do not exceed 0.46 *apfu*, pointing towards the Alkali tourmaline subgroup (Fig. 8A).

Dominant divalent cations in the Y-site positions are Fe and Mg. Their concentrations as well as the $Mg/(Mg+Fe_{tot})$ ratio values vary in the range of 0.3–0.8. Therefore, the analysed tourmalines can be attributed to the schorl-dravite series (Fig. 8B).

Characteristic for the studied tourmalines are common growth zonations (Fig. 7B–G). Inclusions, mainly of zircon, rutile, and xenotime are also a quite common feature in the analysed tourmalines (Fig. 7H).

We used the provenance $Al–Fe_{tot50}Al_{50}–Mg_{50}Al_{50}$ and $Ca–Fe_{tot}–Mg$ diagrams (Henry & Guidotti 1985), where, based on relative contents of the four most important substituent elements namely Al, Fe, Mg, and Ca, it is possible to distinguish several various parent rock types (Fig. 9). The analysed detrital tourmalines were derived mainly from metapelites or metapsamites and only few can be linked to granitoid rocks and associated pegmatites.

Based on the Fe# value it is possible to discriminate tourmalines derived from granitoid rocks (0.8–1.0), hydrothermal vein systems, or metasedimentary rocks (0.4–0.6) (Henry & Guidotti 1985; Henry & Dutrow 1996). The Fe# of the analysed detrital tourmalines varies in the range of 0.31–0.83.

Chemistry of detrital garnets

The analysed detrital garnets show considerable variations in the chemical composition (Fig. 10, Suppl. Table S3). According to the chemical variations, the analysed garnets can be divided into six different groups:

- The first group is represented by garnets with a high content of the pyrope molecule (25–37 mol. %), a high content of grossular (18–24 mol. %) and almandine (43–53 mol. %) and a low content of spessartine (<2 mol. %).
- Garnets belonging to the second group are characterized by a high content of pyrope (39 mol. %) and almandine (56 mol. %) and low contents of the grossular (3 mol. %) and spessartine (~1 mol. %) molecules.
- The third group of garnets is characterized by a high content of almandine (66–74 mol. %), a moderate content of pyrope

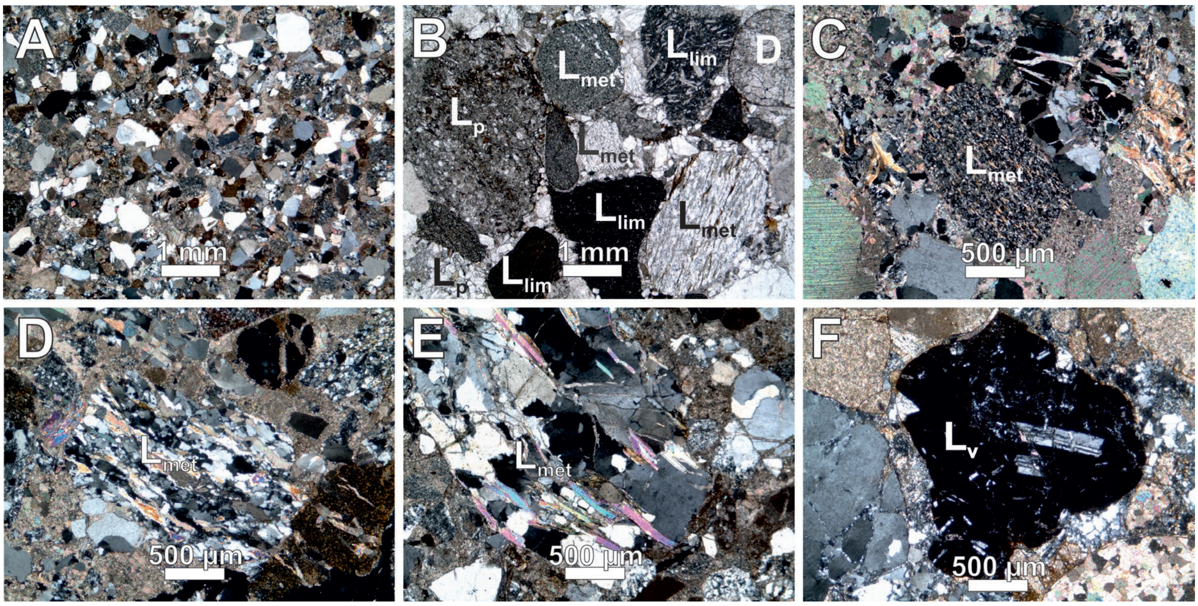

Fig. 5. Types of lithoclasts of the JPF: **A** — medium-grained quartzo–lithic arenite; **B** — coarse-grained sandstone to fine-grained conglomerate composed of lithoclasts of limestones (L_{lim}), dolomites (D), psephitic and psammitic clastic rocks (L_p) and metamorphic rocks (L_{met}); **C–E** — lithoclasts of metamorphic rocks; **F** — clast of a basic volcanic rock. All photographs taken under crossed polars.

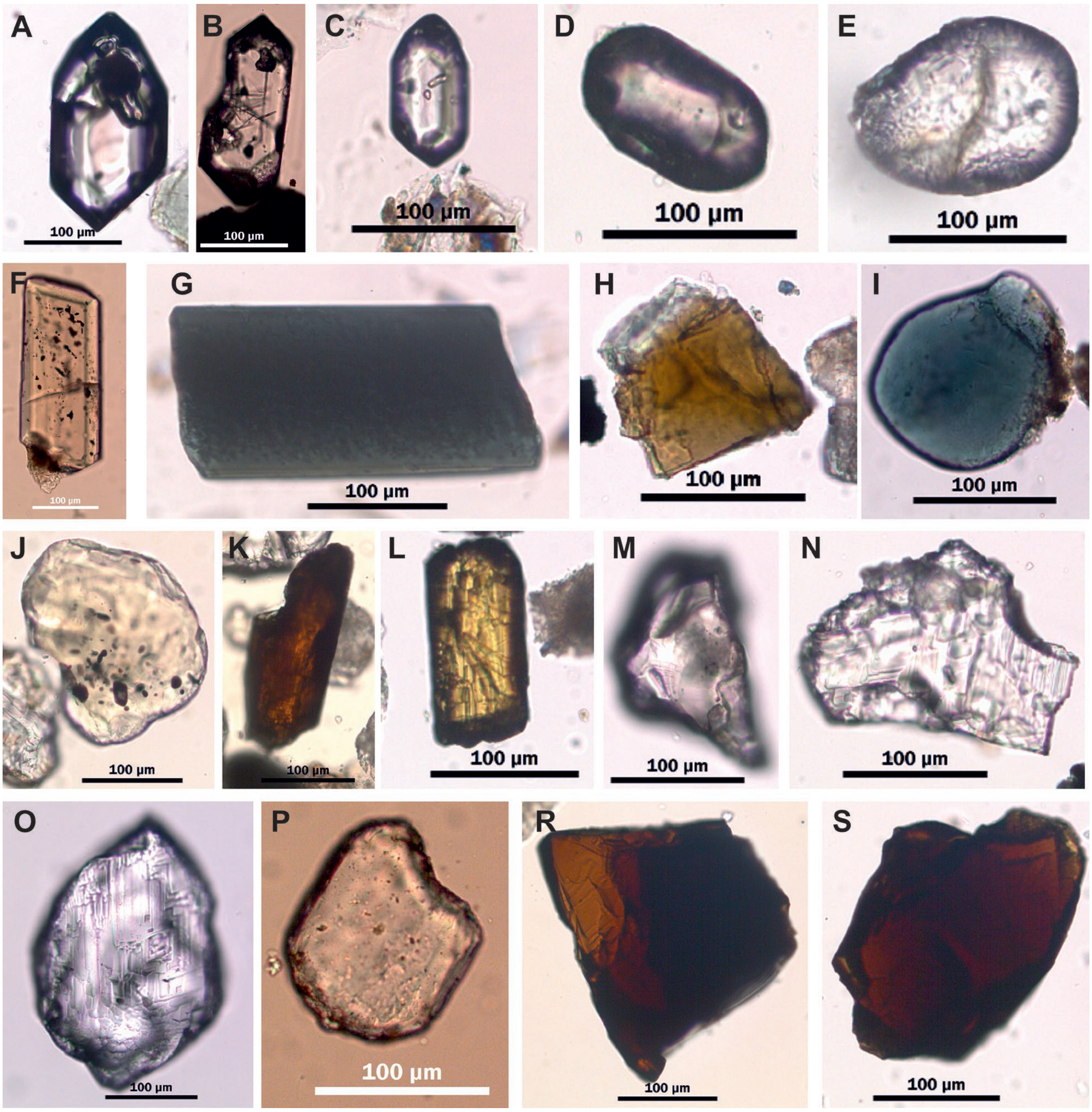

Fig. 6. Characteristic heavy minerals selected from the sediments studied: **A–E** — colourless euhedral to rounded zircons with inclusions; **F** — euhedral tourmaline; **G** — broken prisms of subhedral tourmaline; **H** — initial to advanced features of corrosion around rims of angular tourmaline; **I, J** — variously coloured rounded tourmalines; **K, L** — orange and lemon yellow subrounded rutiles; **M–O** — colourless angular to subrounded garnets with facets on the surface of grains; **P** — subrounded apatite; **R, S** — grains of unaltered fresh Cr-spinels.

(16–27 mol. %), and low grossular (<4 mol. %) and spessartine (<7 mol. %) contents.

- The fourth group is represented by a low content of spessartine molecule (8 mol. %) and lower content of almandine (54 mol. %) and pyrope (13 mol. %) and a higher content of the grossular molecule (25 mol. %) than the previous group.
- Most of the analysed garnets have a high content of the almandine molecule (46–82 mol. %), a variable content of spessartine (1–50 mol. %), low pyrope (<14 mol. %) and low grossular (<11 mol. %) contents.
- The last group is represented by garnets with the slightly lower content of almandine (35–74 mol. %) and spessartine (<37 mol. %) and higher content of grossular (14–26 mol. %) than the previous group, while the content of pyrope is low (<6 mol. %).

All of the analysed garnets contain very low uvarovite and andradite amounts of <0.3 mol. % and <3 mol. %, respectively.

Inclusions in the analysed garnets are most often represented by quartz, epidote and biotite (Fig. 7I–L).

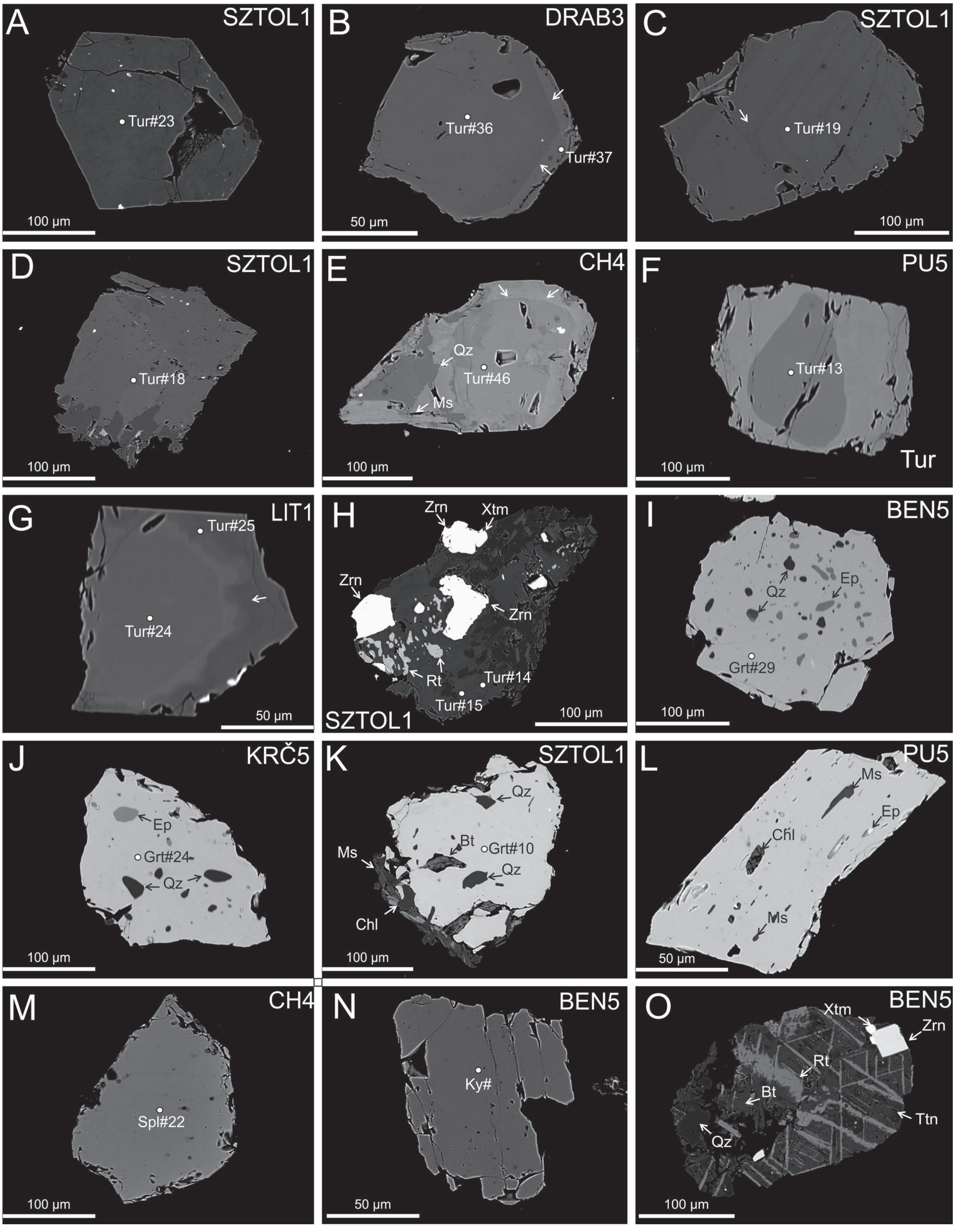

Fig. 7. Back-scattered electron (BSE) images of the separated detrital heavy minerals for the mineral chemistry study. Abbreviations of minerals (Whitney & Evans 2010): Qz — quartz, Bt — biotite, Ms — muscovite, Chl — chlorite, Xtm — xenotime, Ky — kyanite, Ep — epidote. Explanations: Grt#24, Tur#36 — numbers of the analyses in the Supplement.

Chemistry of detrital Cr-spinels

Based on the variability of the TiO_2 content and the Fe^{2+}/Fe^{3+} ratio it is possible to distinguish the upper mantle or volcanic origin of spinels (Lenaz et al. 2000; Kamenetsky et al. 2001). Upper mantle spinels are generally characterized by a low TiO_2 content (<0.2 wt. %). Their Fe^{2+}/Fe^{3+} ratio is higher than two (>2), within the overall range of Al_2O_3. Volcanic spinels exhibit low TiO_2 value only in very rare cases (e.g., some low TiO_2 MORB basalts, tholeiites or boninites, Kamenetsky et al. 2001). The amount of TiO_2 of the analysed spinels varies in the range of 0.02–0.31 wt. % (Suppl. Table S4). A few spinels show higher TiO_2 contents (3.26 wt. %), but it is rather a reflection of initial alteration phases (the spinels also exhibit low contents of Al_2O_3 and MgO and a higher content of Fe_2O_3) than primary crystallization conditions (cf. Mikuš & Spišiak 2007).

The content of Al_2O_3 in the JPF vary in the range of 6.8–51.6 wt. % (Suppl. Table S4). Contents of TiO_2 and Al_2O_3 in spinels are controlled by the parent magma, so they are good indicators of their parent rocks (Kamenetsky et al. 2001). Based on the content of oxides, sources of upper mantle spinels can be divided into two groups, namely supra-subduction peridotites (SSZ peridotites; low Al_2O_3 content) and MORB peridotites (high Al_2O_3 content) (Fig. 11A). Contents of Cr_2O_3 vary in the JPF in the range of 17.6–55.7 wt. %. (Suppl. Table S4).

Most of the spinels show values of the Cr#=(Cr/Cr+Al) and the Mg#=(Mg/Mg+Fe^{2+}) in the range of 50–80 mol. % and 39–70 mol. %, respectively. According to the Cr# and Mg#, the analysed spinels belong to mantle peridotites (Lenaz et al. 2000). In the Cr# vs. Mg# discrimination diagram (Dick & Bullen 1984; Pober & Faupl 1988) (Fig. 12), the analysed spinels mainly plot in the central area of the diagram, where the fields largely overlap. A large majority of the analysed spinels show the Cr# in the range of 50–65, which is adequate to the type II peridotites (harzburgites). Some of the spinels of the JPF show lower values of the Cr# and higher values of the Mg#, including them in the type I peridotites (lherzolites) (Dick & Bullen 1984) (Fig. 12).

Besides the low TiO_2, the analysed spinels are also characterized by the low Fe^{3+} and by variable contents of Cr and Al. In the ternary Cr–Al–Fe^{3+} diagram (Fig. 11B), almost all spinels plot along a Cr–Al trend. The Cr–Al trend is defined as a relation of the Cr/(Cr+Al) vs. Fe^{2+}/(Mg+Fe^{2+}) typical for mantle and lower crustal rocks (e.g., upper mantle xenoliths, ophiolites, mid-ocean peridotites) (Barnes & Roeder 2001).

Discussion

Modal composition and heavy mineral assemblage

The modal composition of the studied sandstones suggests their supracrustal provenance. The high amount of carbonate clastic material, the low feldspar and the low volcanic clast content together with the character of metamorphic clasts point to a source area composed mainly of carbonate sedimentary rocks and low- to medium-grade metamorphic rocks. According to the discrimination diagrams of Dickinson & Suczek (1979) and Dickinson (1985) such compositions are related to source areas of a recycled collisional orogen (Fig. 4). In our case the Q_mFL_t diagram seems to be more appropriate than the QFL diagram of Dickinson (1985) since a consideration of carbonate clasts to the L pole lead to an undissected arc provenance (cf. von Eynatten & Gaupp 1999). Because the sandstone composition is size dependent (Ingersoll et al. 1984), the individual size fractions were plotted separately (Figs. 3, 4). The medium-grained sandstones plot closer to

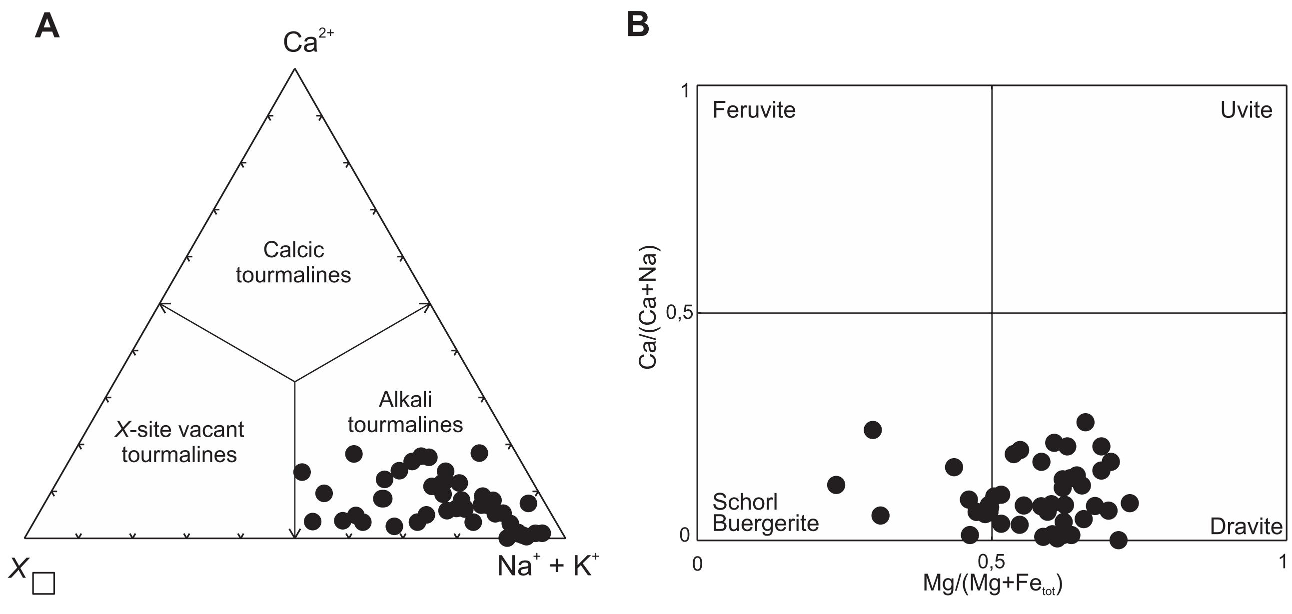

Fig. 8. Classification of basic tourmaline groups; based on dominant occupancy at the X-site (Henry et al. 2011).

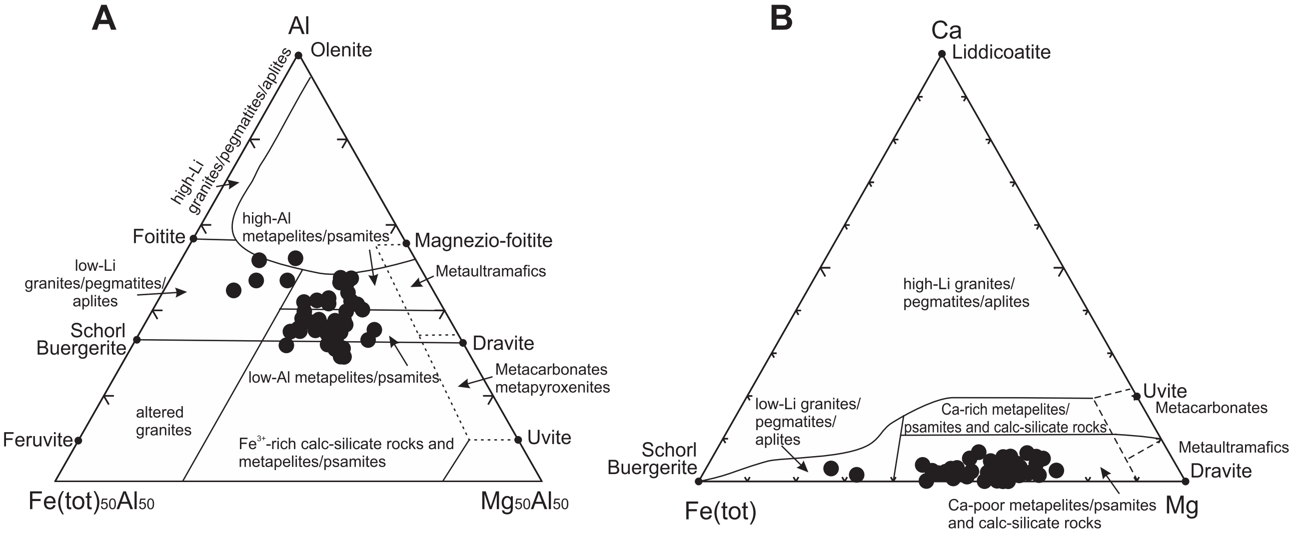

Fig. 9. Compositional provenance diagrams for tourmalines: **A** — ternary Al–$Fe_{(tot)}$–Mg diagram; **B** — ternary Ca–$Fe_{(tot)}$–Mg diagram (Henry & Guidotti 1985).

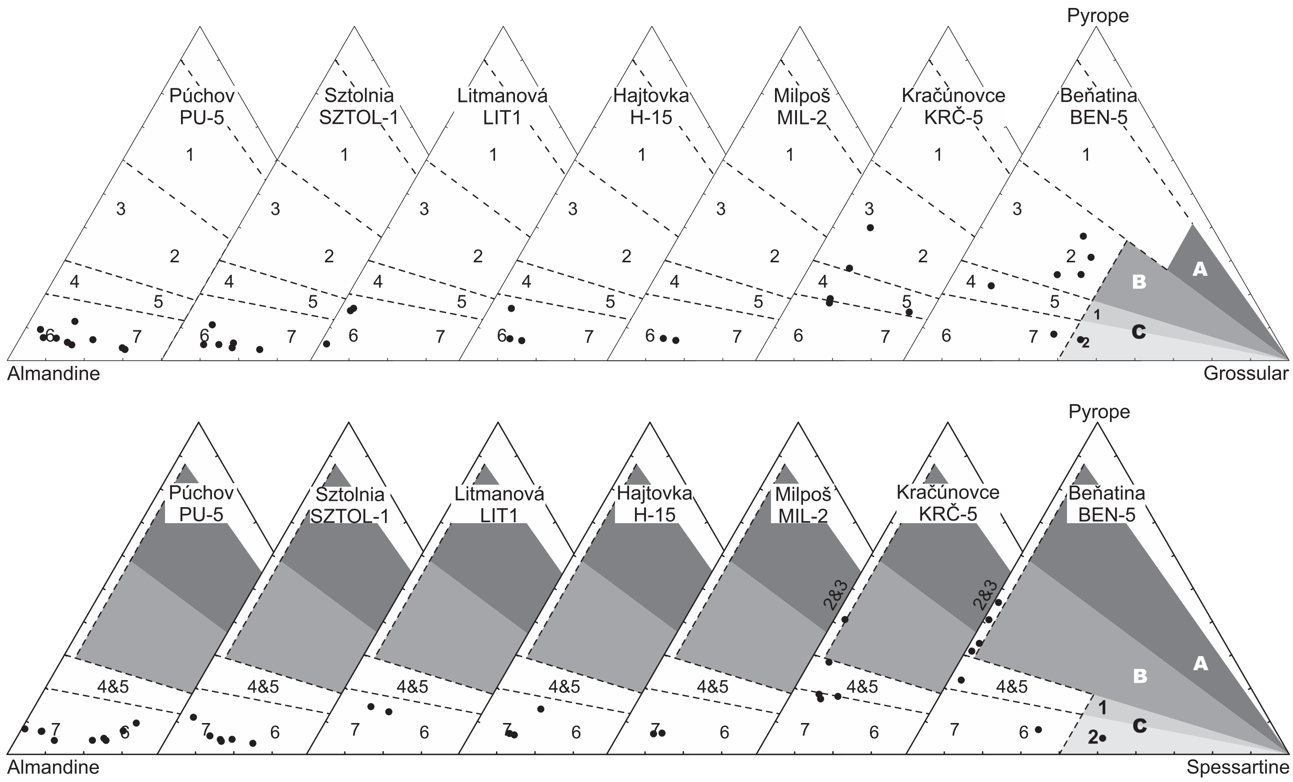

Fig. 10. Ternary pyrope–almandine–grossular and pyrope–almandine–spessartine provenance diagrams (Méres 2008; Aubrecht et al. 2009). Explanations: A — Grt derived from UHP/HP metamorphic conditions; position around number 1 — Grt derived from UHP eclogites, garnet peridotites and kimberlites; B — Grt derived from granulite and eclogite facies conditions; position around number 2 — Grt derived from HP eclogites and HP mafic granulites; position around number 3 — Grt derived from HP felsic and intermediate granulites; C — Grt derived from amphibolite facies conditions; C1 — Grt derived from transitional high amphibolite to granulite facies conditions; position around number 4 — Grt derived from gneisses metamorphosed under transitional high amphibolite to granulite facies conditions; position around number 5 — Grt derived from amphibolites metamorphosed under transitional high amphibolite to granulite facies conditions; C2 — Grt derived from amphibolite facies conditions; position around number 6 — Grt from gneisses metamorphosed under amhibolite facies conditions; position around number 7 — Grt from amphibolites metamorphosed under amphibolite facies conditions. Grey fields — immiscibility gap of end members composition.

the Q pole than coarse-grained sandstones, reflecting their more distal deposition from the source, low resistance of carbonate clasts and/or disintegration of polycrystalline quartz aggregates into monocrystalline quartz grains due to mechanical abrasion during transport.

Collisional orogens provide huge amounts of detrital material derived from a great variety of rock types and multiple recycling of variegated material from older sedimentary formations incorporated into a prograding orogenic wedge. The ratio of ultrastable zircon, tourmaline and rutile to all transparent heavy minerals in siltstones/sandstones, i.e. the ZTR index, is used to get information about a possible recycling of clastic material and maturity of sediments (Hubert 1962). The ZTR index in the studied sandstones ranges from 18 to 73 (Table 2). Accordingly, considerable amounts of the detrital material could have been recycled from older sedimentary formations. On the other hand, the prevalence of euhedral to subhedral habit of ultrastable heavy minerals combined with a high proportion of lithic carbonate clasts suggest rather local sources and a relatively shorter transport. Consequently, the modal composition of the studied sediments, together with the heavy mineral assemblage, points to a mixed provenance of the detrital material, but still from local sources. One source can be determined by the presence of the first-cycle derived carbonate material, poor-rounded ZTR, Grt and Cr-spinels. Another source can be deduced by the presence of the well-rounded resistant clastic material coupled with the subrounded to rounded ultrastable ZTR and Cr-spinels delivered from older sedimentary formations.

As the less stable mineral phases such as epidote and sphene were identified, though in a minor amount, a more diverse original heavy mineral assemblage might be assumed. Less stable minerals were most probably eliminated due to mechanical abrasion and weathering during transport and/or intrastratal dissolution during burial diagenesis (Morton & Hallswoth 1999, 2007; Turner & Morton 2007).

Origin of detrital tourmalines

The chemical composition of analysed detrital tourmalines reveals their derivation mostly from low- to medium-grade metamorphic rocks and to a lesser extent from granitoid rocks (Fig. 9). A similar chemical composition of detrital tourmalines has been reported from the Lower Jurassic deposits of the PKB in the Orava region and from the Lower Jurassic deposits of the Tatric Unit of the CWC in the Malé Karpaty Mts. (Aubrecht 1994; Aubrecht & Krištín 1995). A very large amount of the detrital tourmalines in deposits of the Klape and Manín units were derived, besides metasediments, also from granitoid rocks (Aubrecht 2001). It has been hypothesized that a source of the tourmalines might have been an area composed of metamorphic and granitoid rocks, situated to the north of the Tatric realm, supplying detrital material to both the Lower Jurassic Tatric deposits to the south and to the Lower Jurassic Oravic deposits to the north (Aubrecht 2001). The sources of detrital tourmalines were also assumed to be in metamorphic rocks of the CWC tectonic units, but because of either the very low concentration of tourmalines in that rocks or a considerably large distance to the final deposition place, these sources seem to be very unlikely (cf. Aubrecht 1994; Aubrecht & Krištín 1995 and references therein). If we assume crystalline rocks of the CWC as the source of detrital tourmalines, they should have experienced several sedimentary cycles, resulting in a more advanced rounding of detrital grains, which is not the case. For example, compositionally similar but predominantly well-rounded tourmalines have been reported from

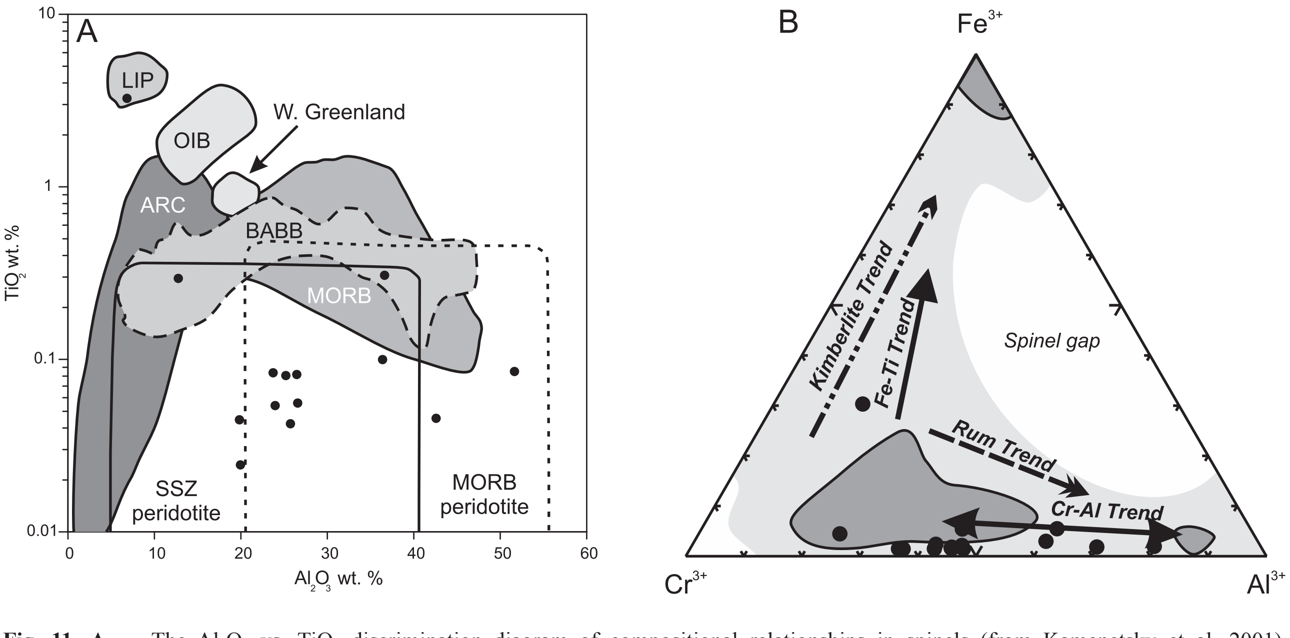

Fig. 11. A — The Al_2O_3 vs. TiO_2 discrimination diagram of compositional relationships in spinels (from Kamenetsky et al. 2001). **B** — The Cr–Al–Fe^{3+} ternary plot with the main relationship trends in spinel compositions (spinel gap field after Barnes & Roeder 2001).

Upper Cretaceous and Oligocene flysch deposits of the EWC (Salata & Uchman 2013; Salata 2014). Crystalline rocks of the Bohemian Massif and/or basement rocks of Brunovistulicum have been interpreted as their primary sources. These rocks had supplied the Upper Palaeozoic and partly Mesozoic clastic rocks deposited on the Silesia and Małopolska blocks, later becoming the ultimate source for flysch deposits of the Skole Basin (Salata 2014). Consequently, the majority of detrital tourmalines in clastic deposits of the PKB units were most probably derived from primary source rocks situated in more proximal areas represented by supracrustal, mainly low- to medium-grade metamorphic rocks either of the Oravic ribbon continent or more external parts of the CWC (cf. Aubrecht 2001).

Origin of detrital garnets

Detrital garnets from the studied rocks exhibit a considerable variability of chemical composition suggesting their origin in various parent rocks types. The analysed garnets were derived mainly from amphibolite metamorphic facies rocks, transitional amphibolite to granulite facies rocks or from retrograde eclogites, and from HP/HT granulites and eclogites.

At five studied localities, almandine type garnets prevail. They were most probably derived from gneisses and amphibolites originated under amphibolite facies metamorphic conditions. Garnets of this composition were also reported from HP/LT metamorphic rocks and metabasic rocks (blueschist facies rocks), skarns, contact metamorphic rocks, migmatites and various types of granitoid rocks (see Méres 2008; Aubrecht et al. 2009). However, we have not observed index minerals of HP/LT metamorphism. Detrital garnets, dominantly of almandine composition, have also been reported from the Maastrichtian–Palaeocene Jarmuta Fm. of the Grajcarek Unit and from the Coniacian–Santonian Sromowce Fm. of the Branisko Unit of the PKB in Poland (Salata 2004). Detrital garnets of a similar composition also occur in Jurassic deposits of the CWC nappe units. Their source rocks have been regarded as low- to medium-grade metamorphic rocks of the CWC crystalline basement (Aubrecht & Méres 2000).

At the two localities from the eastern part of the PKB, detrital garnets with a higher content of the pyrope molecule (<39 %) were revealed in the heavy mineral assemblage (Suppl. Table S3). The chemical composition of these garnets suggests their derivation from granulites (Fig. 10 sector C1

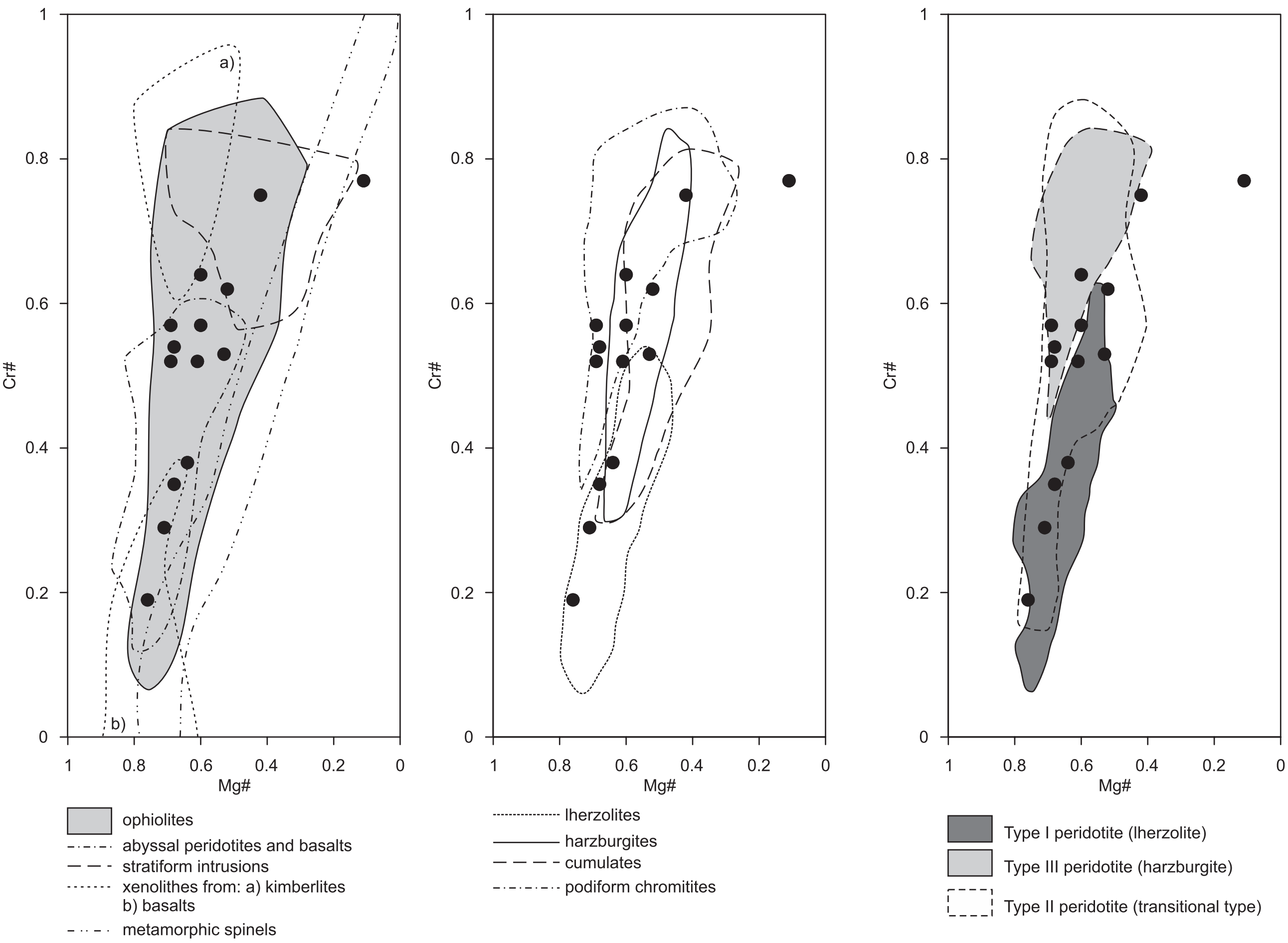

Fig. 12. The Cr# vs. Mg# bivariate plots of calculated cation ratios Cr/(Cr+Al) vs. Mg/(Mg+Fe^{2+}) (the discrimination fields after Dick & Bullen 1984; Pober & Faupl 1988).

number 4) and amphibolites and/or retrograde eclogites metamorphosed under transitional amphibolite to granulite facies conditions (Fig. 10 sector C1 number 5). Garnets with a high content of pyrope and grossular and with a low content of spessartine were derived from eclogites or mafic granulites (Fig. 10 sector B number 2). Garnets with a high content of pyrope and almandine but a low content of grossular and spessartine originated in felsic to intermediate granulites (Fig. 10 sector B around number 3). Garnets of similar composition (pyrope–almandine and pyrope–almandine–grossular) prevail in heavy mineral assemblages of Jurassic deposits (Aubrecht & Méres 2000) and also in the Albian deposits of the Czorsztyn succession of the PKB (Aubrecht et al. 2009). They have also been reported in the Cretaceous and Palaeogene flysch deposits of the EWC (Otava et al. 1998; Salata 2004; Oszczypko & Salata 2005; Grzebyk & Leszczyński 2006). There is a lack of pyrope–almandine garnets in crystalline basement rocks of the CWC and Internal WC (IWC) (Aubrecht & Méres 2000 and references therein). Accordingly, the HP/HT granulite and eclogite facies rocks of the ancient Oravic ribbon continent (or Czorsztyn Ridge) are assumed to have been a source of pyrope–almandine garnets within the Jurassic and Cretaceous sediments of the PKB. This continental fragment was derived, most probably, from the Moldanubian Zone of the Bohemian Massif by rifting during the Middle Jurassic (Aubrecht & Méres 2000; Aubrecht et al. 2009).

Another explanation, which should be taken into consideration, is that high-pyrope garnets could have been derived from sub-ophiolitic high-grade metamorphic soles developed in SSZ settings of the Meliata–Vardar oceanic realm (e.g., Lužar-Oberiter et al. 2008; Mikes et al. 2008; Stern & Wagreich 2013). The dominance of mostly harzburgitic (SSZ peridotites) detrital Cr-spinels may support this model.

As indicated by generally poor roundness of detrital garnets, a more proximal primary source should be assumed. The high-pyrope garnets could have been derived from HT/HP felsic or mafic granulite and eclogite facies rocks of a lower crust exhumed during formation of the Vahic oceanic basin, which were later incorporated into the prograding CWC orogenic wedge in the uppermost Cretaceous to Palaeogene times. Palaeotransport directions reported from the Jarmuta Fm. in the Polish part of the PKB show that detrital material was delivered mainly from SE (Salata 2004; Oszczypko & Salata 2005). Unfortunately, palaeotransport directions collected during our study could not be used for the identification of source areas due to poor outcrop conditions and problematic tectonic restoration. Nevertheless, our measured data roughly agree with the palaeotransport of detrital material from SE towards NW. However, the reported palaeocurrent data have not been corrected for the Miocene united ~50–60° counterclockwise (CCW) rotation of the Alcapa block revealed by the palaeomagnetic studies of the Flysch Belt, PKB and Central Carpathian Palaeogene Basin (Márton et al. 2009a, b, 2013). If the Miocene CCW rotation is taken into account a general palaeotransport of detrital material from S/SWS towards N/NEN is indicated (Fig. 13).

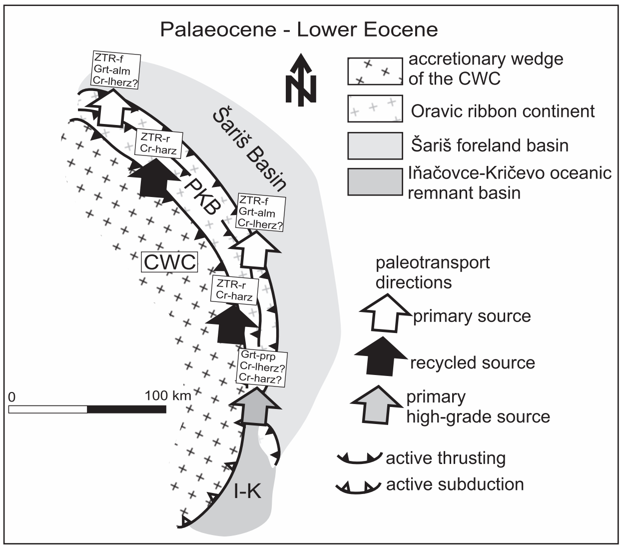

Fig. 13. Schematic palaeogeographic situation of the Pieniny Klippen Belt during Palaeocene–Lower Eocene (based on Soták et al. 1994, 2005; Plašienka & Soták 2015; Kováč et al. 2016). CWC — Central Western Carpathians; PKB — PieninyKlippen Belt; I–K — Iňačovce–Kričevo remnant oceanic basin; ZTR-f — first-cycle poor-rounded ultrastable minerals; ZTR-r — recycled well-rounded ultrastable minerals; Grt-alm — almandine garnets from low- to medium-grade metamorphic rocks; Grt-prp — pyrope–almandine garnets from high-grade metamorphic rocks; Cr-harz — Cr-spinels of harzburgitic origin; Cr-lherz — Cr-spinels of lherzolitic origin

In the eastern part of the WC, the continuation of the Vahic oceanic system is thought to be the Iňačovce–Kričevo remnant oceanic basin (Soták et al. 1993, 1994, 2005; Plašienka & Soták 2015; Kováč et al. 2016). While subduction of the Vahic oceanic or thinned continental crust ceased at the Cretaceous/Palaeogene boundary on the western part of the WC, the Iňačovce–Kričevo remnant basin was still active till the end of the Eocene on the east (Soták et al. 1994, 2005; Kováč et al. 2016). Therefore, this southerly situated realm (before Miocene rotation) could have provided a source of high-pyrope garnets (Fig. 13). In the western part of the PKB, these sources were already eroded and did not exist during deposition of the JPF, since it contains only almandine garnets derived from accreted low- to medium-grade metamorphic rocks of the Oravic ribbon continent.

Origin of detrital Cr-spinels

In the PKB s.l., the first occurrence of detrital Cr-spinels has been revealed in the Barremian–Aptian pebble material of the Albian exotic conglomerates of the Klape Unit and in equivalent Coniacian–Santonian conglomerates of the Pieniny Unit (Mišík et al. 1980). A relatively high content of Cr-spinels has been reported from condensed, red marly sediments with clastic admixtures of the Albian Chmielowa Fm. of the Czorsztyn succession (Aubrecht et al. 2009). Significant amounts of Cr-spinels were found in the Upper Cretaceous to Palaeocene flysch deposits of the Grajcarek and Branisko units of the PKB in southern Poland (Winkler & Ślączka 1992, 1994; Salata 2002, 2004; Oszczypko & Salata 2005). The pebble material (Mišík et al. 1991) and sandstones (Bónová et al. 2018) of the Palaeogene Proč Conglomerates from eastern Slovakia contain Cr-spinels as well.

The source of the ophiolitic detritus in clastic deposits of the PKB has been generally considered to be the same as for the material of the exotic conglomerates of the Klape Unit (for comprehensive review see e.g., Mišík & Marschalko 1988; Dal Piaz et al. 1995; Aubrecht et al. 2009; Plašienka 2012a; Plašienka & Soták 2015). An exotic or cryptic (totally destroyed or buried) ridge, known as the Pieniny Ridge (Andrusov 1938, 1945; Mišík & Sýkora 1981; Mišík & Marschalko 1988), or the Andrusov Ridge (Birkenmajer 1988) has been suspected to be the source of the exotic material. The Andrusov Ridge was supposed to occupy the position between the Kysuca–Pieniny (Vahic) sedimentary realm and the external margin of the CWC units forming the accretionary wedge created by the subduction of the Vahic Ocean (sensu Maheľ 1981, 1989; Birkenmajer 1988). Accordingly, the Cr-spinels in clastic sediments of the PKB could represent ophiolitic detritus of the completely consumed Vahic oceanic crust. The Pieniny or Andrusov Ridge was interpreted as a compressional structure (Mišík 1979; Birkenmajer 1988; Maheľ 1989), therefore, it should have been situated on the active continental margin, although that is not in accordance with the Upper Jurassic to Lower Cretaceous structural, magmatic and sedimentary rock record. The Lower Jurassic to Lower Cretaceous period was characterized by an extensional, and not a compressional tectonic regime in the north Tatric realm (Plašienka 1995a, b, 1996). This assumption led to the alternative explanation that the Klape Flysch represents an analogue to the Albian–Cenomanian Poruba Flysch of the Tatric and Fatric units of the CWC. Consequently, the Klape Unit might have been derived from the Fatric Zliechov Basin. Therefore, the variegated detrital material and the ophiolitic detritus could have come from source areas situated near the Veporic Unit being uplifted and eroded due to the closure of the Meliata Ocean in the Late Jurassic (Plašienka 1995a, b, 1996). Subsequently, the nappe transport of the Fatric nappe system over the Tatricum took place in the Turonian and the Klape Unit gravitationally slid down to a false accretionary wedge position externally to the north Tatric margin (Plašienka 1997, 1999, 2012a; Prokešová et al. 2012).

Another interpretation assumes that the Oravic ribbon continent was placed in the lateral continuation of the CWC and IWC units, in a close vicinity to the Meliatic oceanic realm during the Jurassic. Later, during the Early to middle Cretaceous, the Oravic ribbon continent was separated from its original position, and due to a clockwise rotation of the entire CWC (Aubrecht & Túnyi 2001) transported to the front of the CWC, where together with the Meliatic ophiolite fragment formed the Andrusov Ridge (Aubrecht et al. 2009; Bellová et al. 2018). Such an assumed elevation, being created in a transpressional tectonic shear zone instead of the contractional tectonic regime (cf. Marschalko 1986), might have fed detrital material and ophiolitic detritus to both the Klape and Oravic basins as well as to the CWC Tatric and Fatric basins for a long time (Aubrecht et al. 2009). Conversely, there is no structural record of such a huge crustal block transport. Moreover, the assumed palaeogeographical interpretation, where the Oravic tectonic units are turned over 180°, means that no basin existed between the Czorsztyn Ridge and CWC units, while the Kysuca–Pieniny Basin was not connected to the Vahic Basin but to the Magura Basin in a more external position (Aubrecht et al. 2009, their figs. 12, 13).

Several authors proposed a recycling model of exotic pebbles in the Senonian and Palaeogene conglomerates of the WC, whereby most of their material was resedimented from the mid-Cretaceous conglomerates of the Klape Flysch (Birkenmajer 1988; Salaj 1991; Plašienka 1995a, 2012a; Plašienka & Soták 2015; Plašienka et al. 2018). Thus, the same pebble material can be found in the Coniacian–Santonian conglomerates of the Sromowce Formation of the Oravic Pieniny Unit and then, in decreasing amounts, also in the Maastrichtian Jarmuta Fm. and the Palaeogene Proč Fm. of the Šariš Unit. Exotic pebbles have also been reported from the Senonian–Eocene conglomerates of the Gosau Group in western Slovakia. Hence, the problem of the exotic pebble material does not only concern the primary source area, but is also reflected by their presence in units within the PKB covering a time span of ~60 Ma (Plašienka & Soták 2015).

The chemical composition of detrital Cr-spinels of the JPF indicates erosion of a common source composed of a transitional harzburgitic/lherzolitic type (the type II peridotite sensu Dick & Bullen 1984; Pober & Faupl 1988). Chemical compositions of detrital Cr-spinels reported from individual tectonic units of the WC show that there is a clear prevalence of harzburgitic parent rocks. Harzburgites are characteristic for the more southern Meliata–Vardar provenance as has been interpreted from many clastic deposits throughout the Alpine–Carpathian–Dinaridic orogenic system (e.g., Pober & Faupl 1988; Árgyelán 1996; von Eynatten & Gaupp 1999; Lužar-Oberiter et al. 2008, 2012; Mikes et al. 2008; Missoni & Gawlick 2011; Stern & Wagreich 2013; Gawlick et al. 2015). On the other hand, the chemical compositions of Cr-spinels derived from the Meliatic and Penninic ultramafic bodies of the WC and eastern part of the Northern Calcareous Alps (NCA) rather correspond to a lherzolitic composition of rocks (Mikuš & Spišiak 2007). However, large alterations of Cr-spinels due to serpentinization and/or low-grade metamorphism complicating their discrimination were observed (Mikuš & Spišiak 2007; Koppa et al. 2014). Another problem may occur when altered spinels are plotted in the discrimination diagrams of Dick & Bullen (1984) and Kamenetsky et al. (2001). As shown by Mikuš & Spišiak (2007), a number of their analyses plot well within the field of SSZ peridotites or harzburgites (type III peridotites). However, most of the fresh spinels correspond to MORB peridotites or mostly to lherzolites (type I peridotites). If serpentinization has a significant effect on the chemistry of the *in situ* Cr-spinels, this will inevitably impact upon the detrital spinel chemistry. Since provenance studies usually rely on the 63–125 μm size fraction, the context of the grain can be lost, especially in the case, where the entire grain is altered or only an altered fragment is preserved (Mikuš & Spišiak 2007). Problems concerning the validity of Cr-spinels as reliable petrogenetic indicators have also been highlighted in a study on the Rum layered intrusion in Scotland (Power et al. 2000), where detrital spinels separated from sediments of streams draining the ultramafic rocks show considerable enrichment of Cr and Fe at the expense of Al. It is, therefore, highly recommended to use discrimination diagrams with more caution especially in the case of the Cr-spinels with genuine higher Al content, which seem to be less resistant to weathering, transport and diagenetic processes (see also Mikuš & Spišiak 2007; Gawlick et al. 2015; Bónová et al. 2017, 2018; Bellová et al. 2018). Accordingly, it is very difficult to differentiate between Penninic or Meliatic sources of ophiolitic detritus based on the spinel chemistry alone (cf. Pober & Faupl 1988; Stern & Wagreich 2013). Nevertheless, some trend is visible in Cr-spinel compositions throughout the sedimentary sequences of the PKB and CWC. Cr-spinels from the Coniacian–Santonian Sromowce Formation of the Pieniny Unit (our unpublished data) have the same harzburgitic origin as those reported from the Albian–Cenomanian Klape Flysch and analogous Poruba Fm. of the Tatric and Fatric tectonic units (Jablonský et al. 2001; Mikuš et al. 2006; Lenaz et al. 2009; Bellová et al. 2018). This pattern fits very well with the recycling model of the exotic pebble material and ophiolitic detritus originated in more southern Meliatic realms as has been proposed most recently by Plašienka (2012a), Plašienka & Soták (2015) and Plašienka et al. (2018).

The occurrence of lherzolitic Cr-spinels in the Maastrichtian to Lower/Middle Eocene JPF may suggest their delivery from a different ophiolitic sequence, most probably of the Vahic provenance. Similar changes in the proportional composition of detrital Cr-spinels in time and space have been observed in the Gosau Group sediments of the NCA and western part of the WC (Stern & Wagreich 2013). In the Coniacian–Santonian sediments, there is a dominance of harzbugitic over lherzolitic-spinels (75:14). The dominance of harzburgitic Cr-spinels is reduced during Campanian and a considerable input of lherzolitic Cr-spinels is evident (53:41), while in the Maastrichtian–Palaeocene sediments, harzburgitic Cr-spinels dominate once again (63:30). Moreover, from the Campanian onwards, the heavy mineral spectra of the Gosau Group sediments record a dominant switchover from an ophiolite–dominated source area to that composed chiefly of high-grade metamorphic rocks (Wagreich & Faupl 1994; Stern & Wagreich 2013). The closure of the Vahic Ocean and the subsequent collision of the Oravic ribbon continent with the frontal edge of the CWC orogenic wedge has been roughly placed at the Cretaceous/Palaeogene boundary (e.g., Plašienka 1997). Therefore, from the Campanian onwards, obduction and erosion of the Vahic ophiolites of the lherzolitic composition might have taken place. The Penninic (Vahic) oceanic basin formation is associated with the Jurassic to Early Cretaceous extension which led to the exhumation of lower crustal high-grade metamorphic rocks and subcontinental mantle rocks composed mostly of lherzolites (e.g., Froitzheim & Manatschal 1996; Plašienka 2003; Manatschal & Münterer 2009). A lower crust composed of felsic to mafic granulite and eclogite facies rocks might then be a hypothetical source for the high-pyrope garnets revealed in the eastern part of the PKB. The negative correlation between detrital Cr-spinels and garnets (Stern & Wagreich 2013) may also support derivation of garnets rather from lower crustal granulite/eclogite facies rocks than from sub-ophiolitic high-grade metamorphic soles formed in SSZ settings of the more southern Meliatic oceanic realm (e.g., Lužar-Oberiter et al. 2008; Missoni & Gawlick 2011; Gawlick et al. 2015). Although, the negative correlation may reflect the originally very low (~2 %) concentration of Cr-spinels in their parent rocks.

Conclusions

The origin of the synorogenic deposits of the PKB was related to the collision of the ancient passive margins of the Vahic Ocean, namely the Oravic ribbon continent in the more external position and the CWC continental margin in the more internal position. The main aim of this paper was to find out how these deposits, through their composition, record information about sources of detrital material. The main conclusions of this paper are:

- The modal composition of the studied medium- to coarse-grained sandstones of the Maastrichtian to Lower/Middle Eocene Jarmuta–Proč Fm. classifies them mostly as quarzolithic to lithic arenites.
- The character of the detrital material suggests its supracrustal provenance. The high amount of carbonate clastic material, the low feldspar and the low volcanic clast content together with the character of metamorphic clasts point to a source area composed mainly of carbonate sedimentary rocks and low- to medium-grade metamorphic rocks.
- The heavy mineral associations and the habitus of individual heavy minerals point to a mixed provenance. One primary source is revealed by the presence of euhedral to subhedral ultrastable ZTR, angular garnets and Cr-spinels. It suggests erosion of mainly low- to medium-grade metamorphic rocks of the Oravic continental fragment. Another, still local source, can be deduced by the presence of subrounded to rounded ultrastable ZTR and Cr-spinels, recycled from the older exotic conglomerates-bearing Sromowce Fm. of the Pieniny Unit. These two sources can be observed throughout the whole studied part of the PKB.
- The chemistry of detrital tourmalines points to their derivation mainly from low- to medium-grade metasedimentary rocks with a minor contribution of granitoid rocks.
- The chemistry of detrital garnets shows the dominance of almandine garnets derived from various types of low- to medium-grade metamorphic rocks. The presence of high-pyrope garnets in the eastern part of the PKB is striking. The high-pyrope garnets may have originated in high-grade

mafic and felsic granulites and eclogites representing most probably a lower crust exhumed during the formation of the Vahic oceanic basin in Jurassic to Lower Cretaceous times. Later in the Upper Cretaceous to Palaeocene, fragments of the high-grade metamorphic rocks were incorporated into the prograding CWC accretionary wedge and provided local sources for the clastic material.

- The Cr-spinels of the Jarmuta–Proč Fm. suggest a mixed harzburgitic and lherzolitic provenance. The harzburgitic Cr-spinels might have been recycled from older exotic conglomerates of the Sromowce Fm. and Klape Flysch, thereby representing ophiolitic detritus of the Upper Triassic–Jurassic Meliata–Vardar Ocean. The lherzolitic Cr-spinels might represent a new contribution of ophiolitic detritus delivered from the exhumed subcontinental mantle forming the Jurassic–Lower/Middle Cretaceous Vahic oceanic floor.

Acknowledgements: We would like to thank reviewers Dorota Salata and Wolfgang Knierzinger for their critical remarks and useful suggestions, which helped to improve the quality of this paper. The work of managing editor Milan Kohút and handling editor Anna Vozárová is gratefully acknowledged. This work was financially supported by the Slovak Research and Development Agency (projects APVV-0212-12 and APVV-17-0170) and by the VEGA Scientific Agency (projects VEGA 1/0388/10, VEGA 2/0028/17).

References

Andrusov D. 1938: Geological study of the Inner Klippen Belt, Western Carpathians. Part III. (Tectonics). *Rozp. St. geol. Úst. Čs. Republ.* 9, 1–375 (in Czech and French).

Andrusov D. 1945: Geological study of the Klippen Belt in the Western Carpathians. Part IV.: Stratigraphy of Dogerian and Malmian. *Práce Štát. Geol. Úst.* 13, 1–176 (in Slovak).

Andò S., Garzanti E., Padoan M. & Limonta M. 2012: Corrosion of heavy minerals during weathering and diagenesis. A catalog for optical analysis. *Sediment. Geol.* 280, 165–178.

Árgyelán B.G. 1996: Geochemical investigations of detrital chrome spinels as a tool to detect an ophiolitic source area (Gerecse Mts. Hungary). *Acta Geol. Hung.* 39, 341–368.

Aubrecht R. 1994: Heavy mineral analyses from „Tatric“ units of the Malé Karpaty Mountains (Slovakia) and their consequences for Mesozoic palaeogeography and tectonics. *Mitt. Österr. Geol. Gesell.* 86, 121–132.

Aubrecht R. 2001: Jurassic heavy mineral distribution provinces in the Western Carpathians. *Mineralia Slovaca* 33, 473–486.

Aubrecht R. & Krištín J. 1995: Provenance of detrital tourmaline in the Lower Jurassic of the Malé Karpaty Mts. *Mineralia Slovaca* 27, 37–44.

Aubrecht R. & Méres Š. 2000: Exotic detrital pyrope-almandine garnets in the Jurassic sediments of the Pieniny Klippen Belt and Tatric Zone: where did they come from? *Mineralia Slovaca* 32, 17–28.

Aubrecht R. & Túnyi I. 2001: Original orientation of neptunian dykes in the Pieniny Klippen Belt (Western Carpathians): the first results. *Contr. Geophys. Geod.* 31, 3, 557–578.

Aubrecht R., Méres Š., Sýkora M. & Mikuš T. 2009: Provenance of the detrital garnets and spinels from the Albian sediments of the Czorsztyn Unit (Pieniny Klippen Belt, Western Carpathians, Slovakia). *Geol. Carpath.* 60, 463–483.

Barnes S.J. & Roeder P.L. 2001: The range of spinel composition in terrestrial mafic and ultramafic rocks. *J. Petrol.* 42, 2279–2302.

Bellová S., Aubrecht R. & Mikuš T. 2018: First results of systematic provenance analysis of the heavy mineral assemblages from the Albian to Cenomanian exotic flysch deposits of the Klape Unit, Tatricum, Fatricum and some adjacent units. *Acta Geol. Slov.* 10, 1, 45–64.

Bezák V., Broska I., Ivanička J., Reichwalder P., Vozár J., Polák M., Havrila M., Mello J., Biely A., Plašienka D., Potfaj M., Konečný V., Lexa J., Kaličiak M., Žec B., Vass D., Elečko M., Janočko J., Pereszlényi M., Marko F., Maglay J. & Pristaš J. 2004: Tectonic map of Slovak Republic. *MŽP SR ŠGÚDŠ*, Bratislava.

Birkenmajer K. 1977: Jurassic and Cretaceous lithostratigraphic units of the Pieniny Klippen Belt, Carpathians, Poland. *Stud. Geol. Pol.* 45, 1–158.

Birkenmajer K. 1986: Stages of structural evolution of the Pieniny Klippen Belt, Carpathians. *Stud. Geol. Pol.* 88, 7–32.

Birkenmajer K. 1988: Exotic Andrusov Ridge: its role in plate–tectonic evolution of the West Carpathian foldbelt. *Stud. Geol. Pol.* 41, 7–37.

Bónová K., Spišiak J., Bóna J. & Kováčik M. 2017: Chromian spinels from the Magura Unit (Western Carpathians, eastern Slovakia)– their petrogenetic and palaeogeographic implications. *Geol. Quarterly* 61, 1, 3–17.

Bónová K., Mikuš T. & Bóna J. 2018: Is Cr-spinel geochemistry enough for solving the provenance dilemma? Case study from the Palaeogene sandstones of the Western Carpathians (eastern Slovakia). *Minerals* 8, 543.

Dal Piaz G.V., Martin S., Villa M.I., Gosso G. & Marschalko R. 1995: Late Jurassic blueschist pebbles from the Western Carpathian orogenic wedge and paleostructural implications for Western Tethys evolution. *Tectonics* 14, 4, 8974–885.

Dick H.J.B. & Bullen T. 1984: Chromian spinels as a petrogenetic indicator in abyssal and alpine-type peridotites and spatially associated lavas. *Contrib. Mineral. Petrol.* 86, 55–107.

Dickinson W.R. 1985: Interpreting provenance relations from detrital modes of sandstones. In: Zuffa G.G. (Ed.): Provenance of Arenites. *Riedel*, Dordrecht, 333–366.

Dickinson W.R. & Suczek C.A. 1979: Plate tectonics and sandstone compositions. *AAPG Bull.* 63, 2164–2182.

Ďurkovič T. 1972: Sedimentary and petrographical study of the Proč Beds of the Beňatina Flysch in eastern Slovakia. *Geol. práce, Správy* 58, 119–124 (in Slovak).

Froitzheim N. & Manatschal G. 1996: Kinematics of Jurassic rifting, mantle exhumation and passive-margin formation in the Austroalpine and Penninic nappes (eastern Switzerland). *Geol. Soc. Am. Bull.* 108, 9, 1120–1133.

Froitzheim N., Plašienka D. & Schuster R. 2008: Alpine tectonics of the Alps and Western Carpathians. In: McCan T. (Ed.): The Geology of Central Europe. Vol. 2: Mesozoic and Cenozoic. *Geol. Soc. Publ. House*, London, 1141–1232.

Galehouse J.S. 1971: Point counting. In: Carver R.E. (Ed.) Procedures in Sedimentary Petrology. *Wiley InterScience*, New York, 385–407.

Garzanti E. 2016: From static to dynamic provenance analysis — Sedimentary petrology upgraded. *Sediment. Geol.* 336, 3-13.

Garzanti E. & Verzzoli G. 2003: A classification of metamorphic grains in sands based on their composition and grade. *J. Sediment. Res.* 73, 5, 830–837.

Gawlick H.-J., Aubrecht R., Schlagintweit F., Missoni S. & Plašienka D. 2015: Ophiolitic detritus in Kimmeridgian resedimented limestones and its provenance from an eroded obducted ophiolitic nappe stack south of the Northern Calcareous Alps (Austria). *Geol. Carpath.* 66, 6, 473–487.

Grzebyk J. & Leszczyński S. 2006: New data on heavy minerals from the Upper Cretaceous–Palaeogene flysch of the Beskid Śląski Mts. (Polish Carpathians). *Geol. Quarterly* 50, 2, 265–280.

Henry D.J. & Dutrow B. 1996: Metamorphic tourmaline and its petrologic applications. In: Anovitz L.M. & Grew E.S. (Eds.): Boron: Mineralogy, petrology and geochemistry. *Rev. Mineral.* 33, 503–557.

Henry D.J. & Guidotti C.V. 1985: Tourmaline as a petrogenetic indicator mineral: an example from the staurolite-grade metapelites of NW Maine. *Am. Mineral.* 70, 1–15.

Henry D.J., Novák M., Hawthorne F.C., Ertl A., Dutrow B.L., Uher P. & Pezzotta F. 2011: Nomenclature of the tourmaline-supergroup minerals. *Am. Mineral.* 96, 895–913.

Horwitz L. 1932: Compte-rendu des recherches géologiques effectuées en 1931 pour la révision des feuilles Nowy Targ et Szczawnica. *Pos. Nauk. Panst. Inst. Geol.* 33, 61–63 (in Polish with French title).

Hubert F.J. 1962: A zircon–tourmaline–rutile maturity index and the interdependence of the composition of heavy mineral assemblages with the gross composition and texture of sandstones. *J. Sediment. Petrol.* 32, 3, 440–450.

Ingersoll R.V., Bullard T.F., Ford R.L., Grimm J. P. Pickle J.D. & Sares S.W. 1984: The effect of grain size on detrital modes: a test of the Gazzi-Dickinson point-counting method. *J. Sediment. Petrol.* 54, 103–116.

Jablonský J., Sýkora M. & Aubrecht R. 2001: Detrital Cr-spinels in Mesozoic sedimentary rocks of the Western Carpathians (overview of the latest knowledge). *Mineralia Slovaca* 33, 487–498 (in Slovak with English summary).

Jurewicz E. 2005: Geodynamic evolution of the Tatra Mts. and the Pieniny Klippen Belt (Western Carpathians): problems and comments. *Acta Geol. Pol.* 55, 295–338.

Kamenetsky V.S., Crawford A.J. & Meffre S. 2001: Factors controlling chemistry of magmatic spinel: an empirical study of associated olivine, Cr-spinel and melt inclusion from primitive rocks. *J. Petrol.* 42, 655–671.

Koppa M., Koller F. & Putiš M. 2014: Petrology and geochemistry of a peridotite body in Central Carpathian Palaeogene sediments (Sedlice, eastern Slovakia). *Geol. Carpath.* 65, 5, 387–399.

Kováč M., Nagymarosy A., Oszczypko N., Ślączka A., Csontos L., Marunteanu M., Matenco L. & Márton E. 1998: Palinspastic reconstruction of the Carpathian–Pannonian region during the Miocene. In: Rakús M. (Ed.): Geodynamic Development of the Western Carpathians. *GS SR*, Bratislava, 189–217.

Kováč M., Plašienka D., Soták J., Vojtko R., Oszczypko N., Less G., Ćosović V., Fügenschuh B. & Králiková S. 2016: Palaeogene palaeogeography and basin evolution of the Western Carpathians, northern Pannonian domain and adjoining areas. *Global Planet. Change* 140, 9–27.

Kováč P. & Hók J. 1996: Tertiary development of the western part of Klippen Belt. *Slov. Geol. Mag.* 2, 136–149.

Lenaz D., Kamenetsky V.S., Crawford A.J. & Princivalle F. 2000: Melt inclusion in detrital spinel from the SE Alps (Italy–Slovenia): a new approach to provenance studies of sedimentary basins. *Contrib. Mineral. Petrol.* 139, 748–758.

Lenaz D., Mazzoli C., Spišiak J., Princivalle F. & Maritan L. 2009: Detrital Cr-spinel in the Šambron–Kamenica zone (Slovakia): evidence for an ocean-spreading zone in the Northern Vardar suture? *J. Earth. Sci. (Geol. Rundsch.)* 98, 345–355.

Leško B. 1960: Palaeogene of the Klippen Belt in eastern Slovakia. *Geologický sborník* 11, 1, 95–103 (in Slovak).

Łoziński J. 1966: Detrital minerals in flysch sandstones of the Pieniny Klippen Belt and adjacent areas. *Prace geol. PAN Oddział Kraków* 37, 1–57 (in Polish with French summary).

Lužar-Oberiter B., Mikes T., von Eynatten H. & Babić L. 2008: Ophiolitic detritus in Cretaceous formations of the Dinarides (NW Croatia): evidence from Cr-spinel chemistry. *Int J. Earth Sci. (Geol. Rundsch.)* 98, 1097–1108.

Lužar-Oberiter B., Mikes T., Babić L. & von Eynatten H. 2012: Provenance of Cretaceous synorogenic sediments from the NW Dinarides (Croatia). *Swiss J. Geosci.* 105, 377–399.

Maheľ M. 1981: Island character of the Klippen Belt: Vahicum–continuation of the southern Penninicum in the Western Carpathians. *Geol. Zbor.–Geol. Carpath.* 32, 3, 293–305.

Maheľ M. 1986: Geological structure of the Czechoslovak Carpathians, Paleoalpine units 1. *Veda, SAS*, Bratislava, 1–503 (in Slovak).

Maheľ M. 1989: Pieniny Klippen belt from the geodynamic model aspect. *Mineralia Slovaca* 21, 99–108.

Manatschal G. & Münterer O. 2009: A type sequence across an ancient magma-poor ocean-continent transition: the example of the western Alpine Tethys ophiolites. *Tectonophysics* 473, 4–19.

Mange A.M. & Mauer H.F.W. 1992: Heavy minerals in colour. *Chapman and Hall*, London, 1–147.

Marschalko R. 1986: Development and geotectonic importance of Cretaceous Flysch of the Klippen Belt. *Veda, SAS*, Bratislava, 1–137 (in Slovak with English summary).

Márton E., Jeleńska M., Tokarski K.A., Soták J., Kováč M. & Spišiak J. 2009a: Current–independent paleomagnetic declinations in flysch basins: a case study from the Inner Carpathians. *Geodin. Acta* 22, 1–3, 73–82.

Márton E., Rauch-Włodarska M., Krejčí O., Tokarski K.A. & Bubík M. 2009b: An integrated paleomagnetic and AMS study of the Tertiary flysch from the Outer Western Carpathians. *Geophys. J. Int.* 177, 924–940.

Márton E., Grabowski J., Plašienka D., Túnyi I., Krobicki M., Haas J. & Pethe M. 2013: New paleomagnetic results from the Upper Cretaceous red marls of the Pieniny Klippen Belt, Western Carpathians: Evidence for general CCW rotation and implications for the origin of the structural arc formation. *Tectonophysics* 592, 1–13.

Méres Š. 2008: Garnets–an important information resource about source area and parent rocks of siliciclastic sedimentary rocks. In: Jurkovič Ľ. (Ed.): Conference „Cambelove dni 2008", Abstract Book. *Comenius University*, Bratislava, 37–43 (in Slovak with English summary).

Mikes T., Christ D., Petri R., Dunkl I., Frei D., Báldi-Beke M., Reitner J., Wemmer K., Hrvatović H. & von Eynatten H. 2008: Provenance of the Bosnian Flysch. *Swiss J. Geosci.* 101, S31–S54.

Mikuš T. & Spišiak J. 2007: Chemical composition and alteration of Cr-spinels from Meliata and Penninic serpentinized peridotites (Western Carpathians and Eastern Alps). *Geol. Quarterly* 51, 257–270.

Mikuš T., Spišiak J., Sýkora M. & Demko R. 2006: Chemical composition of spinels from Mesozoic alkali basalts of the Western Carpathians–implications for sources of detrital spinels in flysch sediments. *Geol. Carpath.* 57, 6, 447–460.

Missoni S. & Gawlick H.J. 2011: Evidence for Jurassic subduction from the Northern Calcareous Alps (Berchtesgaden; Austroalpine, Germany). *Int. J. Earth Sci.* 100, 1605–1631.

Mišík M. 1979: Pieniny Klippen belt and the global tectonics model. In: Maheľ, M. & Reichwalder P., (Eds.): Czechoslovak geology and global tectonics. *Veda, SAS*, Bratislava, 89–102.

Mišík M. 1997: The Slovak part of the Pieniny Klippen Belt after the pioneering works of D. Andrusov. *Geol. Carpath.* 48, 4, 209–220.

Mišík M. & Marschalko R. 1988: Exotic conglomerates in flysch sequences: Examples from the West Carpathians. In: Rakús M., Dercourt J. & Nairn E.M.A. (Eds.): Evolution of the northern margin of Tethys. Vol. 1. *Mém. Soc. Géol. France, Paris, Nouvelle Série* 154, 95–113.

Mišík M. & Sýkora M. 1981: Pieniny exotic ridge reconstructed from pebbles of carbonate rocks of Cretaceous conglomerates of the Pieniny Klippen Belt and Manín Unit. *Záp. Karpaty, Geológia* 7, 7–111 (in Slovak with English summary).

Mišík M., Jablonský J., Fejdi P. & Sýkora M. 1980: Chromian and ferrian spinels from Cretaceous sediments of the Western Carpathians. *Mineralia Slovaca* 12, 209–228.

Mišík M., Sýkora M., Mock R. & Jablonský J. 1991: Palaeogene Proč Conglomerates of the Klippen Belt in the Western Carpathians, material from Neopieninic exotic ridge. *Acta Geol. Geogr. Univ. Comen., Geologica* 46, 1–101.

Morton A.C. & Hallsworth C.R. 1999: Processes controling the composition of heavy mineral assemblages in sandstones. *Sediment. Geol.* 124, 3-29.

Morton A.C. & Hallsworth C.R. 2007: Stability of detrital heavy minerals during diagenesis. In: Mange M.A. & Wright D.T. (Eds.): Heavy Minerals in Use. *Developments in Sedimentology* 58, *Elsevier*, Amsterdam, 433–435.

Nemčok J., Kulmanová A. & Ďurkovič T. 1989: Development and stratigraphic position of the Gregorianka Breccia of the Klippen Belt in eastern Slovakia. *Geol. práce, Správy* 89, 11–37 (in Slovak).

Oszczypko N. & Salata D. 2005: Provenance analyses of the Late Cretaceous–Palaoecene deposits of the Magura basin (Polish Western Carpathians) — evidence from a study of heavy minerals. *Acta Geol. Pol.* 55, 3, 237–267.

Oszczypko N., Ślączka A., Oszczypko-Clowes M. & Olszewska B. 2015: Where was the Magura Ocean? *Acta Geol. Pol.* 65, 319–344.

Otava J., Sulovský P. & Krejčí O. 1998: The results of chemistry of detrital garnets from the Cretaceous sediments of the Rača Unit, Magura Goup. *Geol. Výzk. Mor. Slez.* 4, 29–31 (in Czech).

Ožvoldová L., Jablonský J. & Frantová L. 2000: Upper Jurassic radiolarites of the Czertezik succession and comparison with the Kysuca succession in the east-Slovak part of the Pieniny Klippen Belt (Western Carpathians, Slovakia). *Geol. Carpath.* 51, 2, 109–119.

Pettijohn F.J., Potter P.E. & Siever R. 1972: Sand and sandstone. *Springer-Verlag*, New York, 1–618.

Plašienka D. 1995a: Passive and active margin history of the northern Tatricum (Western Carpathians, Slovakia). *Geol. Rundsch.* 84, 748–760.

Plašienka D. 1995b: Mesozoic evolution of Tatric units in the Malé Karpaty and Považský Inovec Mts.: implications for the position of the Klape and related units in Western Slovakia. *Geol. Carpath.* 46, 2, 101–112.

Plašienka D. 1996: Cryptic ridges or collision orogenic belts? *Mineralia Slovaca* 28, 1, 75–79 (in Slovak).

Plašienka D. 1997: Cretaceous tectonochronology of the Central Western Carpathians (Slovakia). *Geol. Carpath.* 48, 2, 99–111.

Plašienka D. 1999: Tectonochronology and paleotectonic model of the Jurassic–Cretaceous evolution of the Central Western Carpathians. *Veda, SAS*, Bratislava, 1–127 (in Slovak with English summary).

Plašienka D. 2003: Dynamics of Mesozoic pre-orogenic rifting in the Western Carpathians. *Mitt. Őster. Geol. Ges.* 94, 79–96.

Plašienka D. 2012a: Jurassic syn-rift and Cretaceous syn-orogenic, coarse-grained deposits related to opening and closure of the Vahic (South Penninic) Ocean in the Western Carpathians — an overview. *Geol. Quarterly* 56, 4, 601–628.

Plašienka D. 2012b: Early stages of structural evolution of the Carpathian Klippen Belt (Slovakian Pieniny sector). *Mineralia Slovaca* 44, 1, 1–16.

Plašienka D. 2018a: Continuity and episodicity in the early Alpine tectonic evolution of the Western Carpathians: How large-scale processes are expressed by the orogenic architecture and rock record data. *Tectonics* 37, 7, 2029–2079.

Plašienka D. 2018b: The Carpathian Klippen Belt and types of its klippen – an attempt at a genetic classification. *Mineralia Slovaca* 49, 1, 1–24.

Plašienka D. & Jurewicz E. 2006: Tectonic evolution of the Pieniny Klippen Belt and its structural relationships to the External and Central Western Carpathians. *Geolines* 20, 106–108.

Plašienka D. & Mikuš V. 2010: Geological setting of the Pieniny and Šariš sectors of the Klippen Belt between Litmanová and Drienica villages in eastern Slovakia. *Mineralia Slovaca* 42, 2, 155–178 (in Slovak with English summary).

Plašienka D. & Soták J. 2015: Evolution of Late Cretaceous–Palaeocene synorogenic basins in the Pieniny Klippen Belt and adjacent zones (Western Carpathians, Slovakia): tectonic controls over a growing orogenic wedge. *An. Soc. Geol. Pol.* 85, 43–76.

Plašienka D., Grecula P., Putiš M., Kováč M. & Hovorka D. 1997: Evolution and structure of the Western Carpathians: an overview. In: Grecula P., Hovorka D. & Putiš M. (Eds): Geological evolution of the Western Carpathians. *Miner. Slov., Monograph*, 1–24.

Plašienka D., Soták J., Jamrichová M., Halásová E., Pivko D., Józsa Š, Madzin J. & Mikuš V. 2012: Structure and evolution of the Pieniny Klippen Belt demonstrated along a section between Jarabina and Litmanová villages in Eastern Slovakia. *Mineralia Slovaca* 44, 1, 17–39.

Plašienka D., Méres Š., Ivan P., Sýkora M., Soták J., Lačný A., Aubrecht R., Bellová S. & Potočný T. 2018: Meliatic blueschists and their detritus in Cretaceous sediments: New data constraining tectonic evolution of the West Carpathians. *Swiss J. Geosci.*, https://doi.org/10.1007/s00015-018-0330-7

Pober E. & Faupl P. 1988: The chemistry of detrital spinels and its application for the geodynamic evolution of the Eastern Alps. *Geol. Rundsch.* 77, 641–670.

Potfaj M. 1993: Position and role of the Biele Karpaty Unit in the Flysch Zone of the Western Carpathians. *Geol. práce, Správy* 98, 55–78 (in Slovak with English summary).

Pouchou J.L. & Pichoir F. 1985: "PAP" (φpZ) procedure for improved quantitative microanalysis. In: Armstrong J.T. (Ed.): Microbeam Analysis. *San Francisco Press*, 104-106.

Power R.M., Pirrie D., Andersen C.Ø.J. & Wheeler D.P. 2000: Testing the validity of chrome spinel chemistry as a provenance and petrogenetic indicator. *Geology* 28, 11, 1027–1030.

Prokešová R., Plašienka D. & Milovský R. 2012: Structural pattern and emplacement mechanism of the Krížna cover nappe (Central Western Carpathians). *Geol. Carpath.* 63, 1, 13–32.

Rakús M. & Hók J. 2005: The Manín and Klape units: Litostratigraphy, tectonic classification, palaeogeographic position and relationship to Vahicum. *Mineralia Slovaca* 37, 9–26. (in Slovak with English summary).

Ratschbacher L., Frisch W., Linzer H.-G., Sperner B., Meschede M., Decker K., Nemčok M., Nemčok J. & Grygar R. 1993: The Pieniny Klippen Belt in the Western Carpathians of northeastern Slovakia: structural evidence for transpression. *Tectonophysics* 226, 471–483.

Salaj J. 1991: Biostratigraphic correlation of Cretaceous flysch formations in the Klippen- and Peri-Klippen zones of the Middle Váh river valley and their paleogeographic-tectonic history. *Mineralia Slovaca* 23, 4, 295–113 (in Slovak with English summary).

Salata D. 2002: Provenance of chromian spinels of the Szczawnica (Magura nappe) and the Jarmuta (Pieniny Klippen Belt) Formations in the light of their chemical compositiiton. Proceedings of XVII. Congress of Carpathian–Balkan Geological Association, Bratislava, September 1st–4th 2002. *Geol. Carpath., Spec. Iss.* 53, 12–13.

Salata D. 2004: Detrital garnets from the Upper Cretaceous–Palaeogene sandstones of the Polish part of the Magura Nappe and the Pieniny Klippen Belt: chemical constrains. *Ann. Soc. Geol. Pol.* 74, 351–364.

Salata D. 2014: Detrital tourmaline as an indicator of source rock lithology: an example from Ropianka and Menilite formations (Skole Nappe, Polish Carpathians). *Geol. Quarterly* 58, 1, 19–30.

Salata D. & Uchman A. 2013: Conventional and high-resolution heavy mineral analyses applied to flysch deposits: comparative provenance studies of the Ropianka (Upper Cretaceous–Palaeocene) and Menilite (Oligocene) formations (Skole Nappe, Polish Carpathians). *Geol. Quarterly* 57, 4, 649–664.

Scheibner E. 1967: Carpathian Klippen Belt. In: Buday T. et al. (Ed.): Regional Geology of ČSSR, Vol. II — Western Carpathians. No. 2, *ÚÚG-Academia*, Praha, 7–105 (in Czech).

Schmid M.S., Bernoulli D., Fügenshuh B., Matenco L., Schefer S., Schuster R., Tichler M. & Ustaszewski K. 2008: The Alpine–Carpathian–Dinaridic orogenic system: correlation and evolution of tectonic units. *Swiss. J. Geosci.* 101, 139–183.

Soták J., Rudinec R. & Spišiak J. 1993: The Penninic "pull-apart" dome in the pre-Neogene basement of the Transcarpathian Depression (eastern Slovakia). *Geol. Carpath.* 44, 11–16.

Soták J., Spišiak J. & Biroň A. 1994 Metamorphic sequences with "Bündnerschiefer" lithology in the pre-Neogene basement of the East Slovakian Basin. *Mitt. Öster. Geol. Ges.* 86, 111–120.

Soták J., Biroň A. Dunkl I., Lebedev V. Magyar J. & Prokešová R. 2005: Synthesis of knowledge about Iňačovce Unit — lithostratigraphic, metamorphic, geochronologic and structural-tectonic data. *Mineralia Slovaca* 37, 209–213 (in Slovak with English abstract).

Starobová M. 1962: Heavy minerals from Magura Flysch and Klippen Belt in eastern Slovakia. *Geol. práce, Zošit* 63, 47–52. (in Czech).

Stern G. & Wagreich M. 2013: Provenance of the Upper Cretaceous to Eocene Gosau Group around and beneath the Vienna Basin (Austria and Slovakia). *Swiss J. Geosci.* 106, 505–527.

Turner G. & Morton A.C. 2007: The effects of burial diagenesis on detrital heavy mineral grain surface textures. In: Mange M.A. & Wright D.T. (Eds.): Heavy Minerals in Use. *Developments in Sedimentology* 58, *Elsevier*, Amsterdam, 393–412.

Vass D., Began A., Gross P., Kahan Š., Krystek I., Köhler E., Lexa J., Nemčok J., Růžička M. & Vaškovský I. 1988: Explanation to map Regional division of Western Carpathians and northern parts of Pannonian Basin in ČSSR 1:500,000. *GÚDŠ*, Bratislava, 1–46 (in Slovak).

von Eynatten H. & Gaupp R. 1999: Provenance of Cretaceous synorogenic sandstones in the Eastern Alps: constraints from framework petrography, heavy mineral analysis and mineral chemistry. *Sediment. Geol.* 124, 81–111.

Wagreich M. & Faupl P. 1994: Palaeogeography and geodynamic evolution of the Gosau Group of the Northern Calcareous Alps (Late Cretaceous, Eastern Alps, Austria). *Palaeogeogr. Palaeoclimatol. Palaeoecol.* 110, 235–254.

Whitney L.D. & Evans W.B. 2010: Abbreviations for names of rock-forming minerals. *Am. Mineral.* 95, 185–187.

Wierzbowski A., Aubrecht R., Krobicki M., Matyja B.A. & Schlögl J. 2004: Stratigraphy and palaeogeographic position of the Jurassic Czertezik succession, Pieniny Klippen Belt (Western Carpathians) of Poland and eastern Slovakia. *Ann. Soc. Geol. Pol.* 74, 237–256.

Winkler Z. & Ślączka A. 1992: Sediment dispersal and provenance in the Silesian, Dukla and Magura nappes (Outer Carpathians, Poland). *Geol. Rundsch.* 2, 371–382.

Winkler Z. & Ślączka A. 1994: A late Cretaceous to Palaeogene geodynamic model for the Western Carpathians in Poland. *Geol. Carpath.* 45, 2, 71–82.

Zuffa G.G. 1985: Optical analyses of arenites: Influence of methodology on compositional results. In: Zuffa G.G. (Ed.) Provenance of arenites. *NATO ASI Series* 148, *Reidel*, Dordtrecht, 165–189.

Supplement

Table S1: Modal composition data from the analysed sandstones. Q_m=monocrystalline qartz; Q_p=polycrystalline quartz; P=plagioclase; K=potassium feldspar; L_{met}=metamorphic clasts; L_v=volcanic clasts; L_{lim}=limestone clasts; D=dolomite clasts; L_p=clasts of non-carbonate sedimentary rocks; total of quartzose grains Q_t=Q_m+Q_p; total of feldspar F=P+K; total of lithic clasts L_t=Q_p+L_{met}+L_v+L_p; L=L_{met}+L_v+L_p; L_s=L_{met}+L_p; total of carbonate clasts L_{carb}=L_{lim}+D; total of lithic clasts+carbonate clasts=L+Lc_{arb}; L_t+L_{carb}; L_s+L_{carb}.

	Jarmuta–Proč Fm.																	
Sample	Q_m	Q_p	P	K	L_{met}	L_v	L_{lim}	D	L_p	Q_t	F	L	L_t	L_s	L_{carb}	L+L_{carb}	L_t+L_{carb}	L_s+L_{carb}
LIT-A10	64.8	11.3	4.2	2.6	0.0	0.3	11.6	0.0	5.2	76.1	6.8	5.5	16.8	5.2	11.6	17.1	28.4	16.8
LIT-A15	17.8	34.6	0.9	2.3	20.6	2.8	10.3	10.7	0.0	52.3	3.3	23.4	57.9	20.6	21.0	44.4	79.0	41.6
LIT-B5	56.4	18.4	5.1	13.2	1.3	0.0	0.0	1.7	3.8	74.8	18.4	5.1	23.5	5.1	1.7	6.8	25.2	6.8
LIT-B8	30.0	33.5	1.3	2.6	18.3	0.4	8.7	3.9	1.3	63.5	3.9	20.0	53.5	19.6	12.6	32.6	66.1	32.2
LIT-B9	13.1	9.5	0.0	1.5	14.6	0.0	31.7	28.6	1.0	22.6	1.5	15.6	25.1	15.6	60.3	75.9	85.4	75.9
LIT-B10	52.8	13.4	0.9	3.7	8.3	0.5	14.4	1.9	4.2	66.2	4.6	13.0	26.4	12.5	16.2	29.2	42.6	28.7
LIT-B11	24.8	22.2	1.7	3.4	18.4	0.4	17.1	9.0	3.0	47.0	5.1	21.8	44.0	21.4	26.1	47.9	70.1	47.4
LIT-B12	23.6	18.9	0.9	0.9	15.5	0.4	33.5	5.6	0.9	42.5	1.7	16.7	35.6	16.3	39.1	55.8	74.7	55.4
LIT-B13	44.3	18.3	0.9	10.4	11.7	0.4	9.1	2.6	2.2	62.6	11.3	14.3	32.6	13.9	11.7	26.1	44.3	25.7
LIT-B14	31.1	32.0	0.0	3.5	14.9	0.4	7.0	10.1	0.9	63.2	3.5	16.2	48.2	15.8	17.1	33.3	65.4	32.9
LIT-B15	16.9	37.3	0.4	3.6	18.2	0.9	8.0	14.2	0.4	54.2	4.0	19.6	56.9	18.7	22.2	41.8	79.1	40.9
LIT-B16	36.2	27.6	2.3	0.9	13.1	0.0	17.2	2.3	0.5	63.8	3.2	13.6	41.2	13.6	19.5	33.0	60.6	33.0
LIT-B17	44.3	20.1	2.0	7.4	8.6	0.4	15.2	1.2	0.8	64.3	9.4	9.8	29.9	9.4	16.4	26.2	46.3	25.8
LIT-B18	34.0	25.3	2.3	2.3	15.5	1.1	11.7	6.4	1.5	59.2	4.5	18.1	43.4	17.0	18.1	36.2	61.5	35.1
LIT-B19	34.5	12.5	0.5	6.0	9.5	2.0	29.0	3.5	2.5	47.0	6.5	14.0	26.5	12.0	32.5	46.5	59.0	44.5
L29	52.2	5.6	1.7	1.7	2.6	0.0	18.5	0.0	17.7	57.8	3.4	20.3	25.9	20.3	18.5	38.8	44.4	38.8
H-1A	42.9	14.2	0.9	2.7	11.0	0.5	25.6	1.4	0.9	57.1	3.7	12.3	26.5	11.9	26.9	39.3	53.4	38.8
H-1B	30.5	30.1	1.8	2.2	16.5	0.7	14.0	2.6	1.5	60.7	4.0	18.8	48.9	18.0	16.5	35.3	65.4	34.6
H-15	22.6	23.8	0.9	1.3	26.4	3.8	15.7	5.5	0.0	46.4	2.1	30.2	54.0	26.4	21.3	51.5	75.3	47.7
SJ-1A	18.7	16.4	1.8	0.4	18.7	1.3	24.9	16.9	0.9	35.1	2.2	20.9	37.3	19.6	41.8	62.7	79.1	61.3
SJ-1B	20.8	31.7	0.0	0.0	2.5	1.7	20.0	21.7	1.7	52.5	0.0	5.8	37.5	4.2	41.7	47.5	79.2	45.8
SJ32-1	14.1	19.0	0.0	2.3	17.5	0.8	31.2	14.8	0.4	33.1	2.3	18.6	37.6	17.9	46.0	64.6	83.7	63.9
SJ32-2	25.3	21.0	1.1	2.2	8.6	3.2	29.0	7.5	2.2	46.2	3.2	14.0	34.9	10.8	36.6	50.5	71.5	47.3
KYJ1A	61.8	18.7	2.8	0.8	4.1	0.4	7.3	2.4	1.6	80.5	3.7	6.1	24.8	5.7	9.8	15.9	34.6	15.4
KYJ1B	28.6	31.5	0.5	1.4	9.4	0.0	12.2	16.4	0.0	60.1	1.9	9.4	40.8	9.4	28.6	38.0	69.5	38.0
KYJ4-1	41.9	23.9	0.0	2.3	4.1	3.6	17.1	6.8	0.5	65.8	2.3	8.1	32.0	4.5	23.9	32.0	55.9	28.4
KYJ4-2	35.7	16.2	0.5	3.3	9.5	1.0	27.1	6.2	0.5	51.9	3.8	11.0	27.1	10.0	33.3	44.3	60.5	43.3
MILPOS-A	30.0	27.4	1.8	7.6	12.6	1.3	8.5	10.3	0.4	57.4	9.4	14.3	41.7	13.0	18.8	33.2	60.5	31.8
MILPOS-B	28.7	22.8	2.1	3.8	11.0	1.7	18.6	11.0	0.4	51.5	5.9	13.1	35.9	11.4	29.5	42.6	65.4	40.9
MILPOS-C	26.4	24.7	6.3	5.6	12.8	2.8	15.3	6.3	0.0	51.0	11.8	15.6	40.3	12.8	21.5	37.2	61.8	34.4
MIL-1A	49.8	10.0	3.5	8.3	5.7	0.9	20.5	0.0	1.3	59.8	11.8	7.9	17.9	7.0	20.5	28.4	38.4	27.5
MIL-1C	52.8	19.1	1.2	1.6	2.8	0.8	18.3	2.0	1.2	72.0	2.8	4.9	24.0	4.1	20.3	25.2	44.3	24.4
MIL-1D	44.6	22.7	1.2	3.3	5.8	0.8	10.7	8.7	2.1	67.4	4.5	8.7	31.4	7.9	19.4	28.1	50.8	27.3
MIL-1E	67.9	8.5	0.8	0.8	3.3	0.4	17.5	0.0	0.8	76.4	1.6	4.5	13.0	4.1	17.5	22.0	30.5	21.5
MIL-2A	56.3	9.7	0.0	1.9	6.8	0.0	20.9	0.0	4.4	66.0	1.9	11.2	20.9	11.2	20.9	32.0	41.7	32.0
MIL-2B	75.2	4.8	1.3	1.3	1.7	0.0	14.8	0.0	0.9	80.0	2.6	2.6	7.4	2.6	14.8	17.4	22.2	17.4
MIL-5A	47.3	16.5	1.2	3.3	6.2	0.8	22.2	2.1	0.4	63.8	4.5	7.4	23.9	6.6	24.3	31.7	48.1	30.9
MIL-5B	42.2	17.1	1.6	2.7	4.7	1.2	25.6	2.7	2.3	59.3	4.3	8.1	25.2	7.0	28.3	36.4	53.5	35.3
MIL-6	24.1	19.9	1.2	3.7	10.4	1.7	28.6	10.4	0.0	44.0	5.0	12.0	32.0	10.4	39.0	51.0	71.0	49.4
DRA-A1	45.0	20.2	0.4	0.0	10.3	0.0	22.7	0.4	0.8	65.3	0.4	11.2	31.4	11.2	23.1	34.3	54.5	34.3
DRA-A2	18.4	15.2	0.0	0.9	11.2	0.0	23.8	30.5	0.0	33.6	0.9	11.2	26.5	11.2	54.3	65.5	80.7	65.5
DRA-A4	53.4	9.2	1.2	0.4	4.4	0.0	29.3	1.2	0.8	62.7	1.6	5.2	14.5	5.2	30.5	35.7	45.0	35.7
DRA-A7	36.9	4.4	2.0	1.5	6.9	0.5	45.3	1.5	1.0	41.4	3.4	8.4	12.8	7.9	46.8	55.2	59.6	54.7
DRA-B1	60.4	15.2	1.4	0.0	3.2	0.4	14.5	0.7	4.2	75.6	1.4	7.8	23.0	7.4	15.2	23.0	38.2	22.6
DRA-B2	59.4	11.3	0.4	2.3	5.6	0.0	16.9	1.9	2.3	70.7	2.6	7.9	19.2	7.9	18.8	26.7	38.0	26.7
DRA-B3	45.7	15.6	1.1	0.7	13.0	0.4	18.1	2.5	2.9	61.2	1.8	16.3	31.9	15.9	20.7	37.0	52.5	36.6
DRA-B4	49.8	13.2	1.3	1.3	12.8	0.4	17.2	2.2	1.8	63.0	2.6	15.0	28.2	14.5	19.4	34.4	47.6	33.9
DRA-B5	53.9	16.0	0.8	1.6	7.4	0.0	16.0	2.7	1.6	69.9	2.3	9.0	25.0	9.0	18.8	27.7	43.8	27.7
DRA-B6	63.6	8.9	2.3	1.2	5.8	0.0	13.6	3.5	1.2	72.5	3.5	7.0	15.9	7.0	17.1	24.0	32.9	24.0
DRA-B7	50.4	15.8	0.9	0.4	12.4	0.0	16.2	2.6	1.3	66.2	1.3	13.7	29.5	13.7	18.8	32.5	48.3	32.5
DRA-B8	48.8	15.2	0.4	1.2	12.8	0.4	16.4	1.6	3.2	64.0	1.6	16.4	31.6	16.0	18.0	34.4	49.6	34.0
DRA-B9	36.0	19.3	0.8	0.8	14.8	0.4	17.8	9.5	0.8	55.3	1.5	15.9	35.2	15.5	27.3	43.2	62.5	42.8
DRA-B10	26.7	25.5	0.0	0.0	14.2	0.8	21.1	11.7	0.0	52.2	0.0	15.0	40.5	14.2	32.8	47.8	73.3	47.0
DRA-B11	24.7	26.4	0.4	0.8	14.6	0.4	18.0	14.6	0.0	51.0	1.3	15.1	41.4	14.6	32.6	47.7	74.1	47.3
DRA-B14	63.1	13.1	0.7	0.7	3.7	0.0	14.2	0.7	3.7	76.1	1.5	7.5	20.5	7.5	14.9	22.4	35.4	22.4
DRA-B16	59.5	14.9	0.4	1.1	7.8	0.4	13.8	0.0	2.2	74.3	1.5	10.4	25.3	10.0	13.8	24.2	39.0	23.8
DRA-B20	60.8	7.8	0.8	2.7	2.0	0.0	19.2	3.5	3.1	68.6	3.5	5.1	12.9	5.1	22.7	27.8	35.7	27.8
TR-3	30.3	17.0	0.0	1.7	12.0	0.0	27.8	10.8	0.4	47.3	1.7	12.4	29.5	12.4	38.6	51.0	68.0	51.0
TR-5A	34.9	15.5	0.0	0.4	7.8	0.0	26.0	14.3	1.2	50.4	0.4	8.9	24.4	8.9	40.3	49.2	64.7	49.2
TR-5B	49.6	11.5	0.8	1.2	6.3	0.4	25.4	4.4	0.4	61.1	2.0	7.1	18.7	6.7	29.8	36.9	48.4	36.5
DEM-4	31.5	21.0	0.7	1.1	9.7	1.5	22.8	10.9	0.7	52.4	1.9	12.0	33.0	10.5	33.7	45.7	66.7	44.2
DEM-5	36.2	23.6	0.0	0.0	7.4	4.4	11.8	16.6	0.0	59.8	0.0	11.8	35.4	7.4	28.4	40.2	63.8	35.8
TUL-3	19.3	4.7	0.5	0.0	1.9	0.5	67.9	4.7	0.5	24.1	0.5	2.8	7.5	2.4	72.6	75.5	80.2	75.0
TUL-4	27.9	7.9	0.5	0.5	6.3	1.6	44.2	11.1	0.0	35.8	1.1	7.9	15.8	6.3	55.3	63.2	71.1	61.6
PU-1	26.5	17.9	0.0	0.0	19.2	3.8	19.7	12.8	0.0	44.4	0.0	23.1	41.0	19.2	32.5	55.6	73.5	51.7
KRC2A	26.1	26.1	0.0	1.4	3.3	0.9	18.5	23.7	0.0	52.1	1.4	4.3	30.3	3.3	42.2	46.4	72.5	45.5
KRC2B	57.5	25.1	1.1	1.1	0.0	0.0	14.0	0.6	0.6	82.7	2.2	0.6	25.7	0.6	14.5	15.1	40.2	15.1
KRC4	3.5	15.3	0.6	1.8	0.0	0.0	41.2	37.6	0.0	18.8	2.4	0.0	15.3	0.0	78.8	78.8	94.1	78.8
KRC5	8.8	24.2	0.0	0.4	0.0	0.9	37.9	27.8	0.0	33.0	0.4	0.9	25.1	0.0	65.6	66.5	90.7	65.6
BEN2	32.4	27.8	0.0	0.0	4.6	0.0	20.4	14.8	0.0	60.2	0.0	4.6	32.4	4.6	35.2	39.8	67.6	39.8
BEN5A	6.4	16.5	0.0	0.0	0.0	1.6	48.9	26.6	0.0	22.9	0.0	1.6	18.1	0.0	75.5	77.1	93.6	75.5
BEN5B	55.4	19.1	0.6	0.6	0.0	1.3	22.9	0.0	0.0	74.5	1.3	1.3	20.4	0.0	22.9	24.2	43.3	22.9

Table S2: Microprobe analyses of detrital tourmalines from the sediments studied.

Formation	JPF													
Sample	PU-5													
Analysis	**Tur#1**	**Tur#2**	**Tur#3**	**Tur#4**	**Tur#5**	**Tur#6**	**Tur#7**	**Tur#8**	**Tur#9**	**Tur#10**	**Tur#11**	**Tur#12**	**Tur#13**	**Tur#14**
SiO_2	36.71	36.59	36.49	36.67	36.94	36.19	36.26	37.56	36.81	36.95	36.01	36.85	36.45	36.61
TiO_2	0.51	0.77	0.76	0.92	0.83	0.65	0.85	0.17	0.11	0.84	0.35	0.56	0.51	0.31
B_2O_3*	10.66	10.70	10.60	10.67	10.80	10.66	10.55	10.92	10.65	10.67	10.38	10.74	10.82	10.54
Al_2O_3	32.32	32.29	31.35	31.35	33.18	34.80	31.40	35.00	30.26	31.09	28.16	32.95	35.92	30.92
Cr_2O_3	0.04	0.05	0.06	0.06	0.07	0.00	0.00	0.06	0.00	0.01	0.00	0.06	0.00	0.01
V_2O_3	0.00	0.00	0.00	0.00	0.00	0.00	0.00	0.00	0.00	0.00	0.00	0.00	0.00	0.00
Fe_2O_3*	0.00	0.00	0.00	0.00	0.00	0.00	0.00	0.00	1.62	0.00	2.80	0.00	0.00	0.00
FeO	9.55	6.68	9.42	7.18	7.40	10.73	9.78	5.22	8.41	8.06	8.79	7.55	8.19	8.43
MnO	0.01	0.01	0.00	0.02	0.03	0.08	0.04	0.01	0.01	0.01	0.02	0.03	0.07	0.01
MgO	5.54	7.27	6.00	7.45	6.35	2.86	5.65	6.93	7.43	7.10	7.11	6.44	4.31	6.98
NiO	0.00	0.02	0.01	0.02	0.00	0.00	0.00	0.01	0.00	0.00	0.00	0.05	0.01	0.00
ZnO	0.00	0.00	0.00	0.00	0.00	0.00	0.00	0.00	0.00	0.00	0.00	0.00	0.00	0.00
CaO	0.34	0.68	0.51	0.99	0.73	0.20	0.37	0.21	0.02	0.40	0.07	0.29	0.22	0.36
Na_2O	2.37	2.25	2.51	2.09	1.93	1.90	2.43	1.66	2.91	2.58	2.76	2.28	1.80	2.44
K_2O	0.02	0.02	0.02	0.01	0.01	0.04	0.02	0.02	0.03	0.02	0.04	0.01	0.05	0.01
H_2O*	3.41	3.37	3.36	3.38	3.34	3.18	3.39	3.51	3.67	3.42	3.58	3.44	3.29	3.53
F	0.00	0.00	0.00	0.00	0.00	0.00	0.00	0.00	0.00	0.00	0.00	0.00	0.00	0.00
Cl	0.01	0.01	0.00	0.01	0.00	0.00	0.00	0.00	0.00	0.00	0.01	0.00	0.04	0.01
Total	101.47	100.70	101.09	100.83	101.60	101.30	100.76	101.28	101.93	101.16	100.09	101.24	101.67	100.14
Si^{4+}	5.98	5.94	5.98	5.97	5.95	5.90	5.97	5.98	6.01	6.02	6.03	5.96	5.86	6.04
Al^{3+}	0.02	0.06	0.02	0.03	0.05	0.10	0.03	0.02	0.00	0.00	0.00	0.04	0.14	0.00
T-sum.	6.00	6.00	6.00	6.00	6.00	6.00	6.00	6.00	6.01	6.02	6.03	6.00	6.00	6.04
B^{3+}	3.00	3.00	3.00	3.00	3.00	3.00	3.00	3.00	3.00	3.00	3.00	3.00	3.00	3.00
Al^{3+}	5.94	5.88	5.90	5.82	5.86	5.96	5.93	5.96	5.82	5.93	5.56	5.94	5.96	5.94
Cr^{3+}	0.00	0.01	0.01	0.01	0.01	0.00	0.00	0.01	0.00	0.00	0.00	0.01	0.00	0.00
V^{3+}	0.00	0.00	0.00	0.00	0.00	0.00	0.00	0.00	0.00	0.00	0.00	0.00	0.00	0.00
Mg^{2+}	0.06	0.12	0.09	0.17	0.13	0.03	0.07	0.04	0.00	0.07	0.01	0.05	0.04	0.06
Fe^{3+}	0.00	0.00	0.00	0.00	0.00	0.00	0.00	0.00	0.17	0.00	0.43	0.00	0.00	0.00
Z-sum.	6.00	6.00	6.00	6.00	6.00	6.00	6.00	6.00	6.00	6.00	6.00	6.00	6.00	6.00
Ti^{4+}	0.06	0.09	0.09	0.11	0.10	0.08	0.11	0.02	0.01	0.10	0.04	0.07	0.06	0.04
Al^{3+}	0.26	0.25	0.14	0.17	0.38	0.62	0.14	0.59	0.00	0.04	0.00	0.31	0.69	0.07
Fe^{3+}	0.00	0.00	0.00	0.00	0.00	0.00	0.00	0.00	0.03	0.00	0.00	0.00	0.00	0.00
Fe^{2+}	1.30	0.91	1.29	0.98	1.00	1.46	1.35	0.70	1.15	1.10	1.16	1.02	1.10	1.16
Mn^{2+}	0.00	0.00	0.00	0.00	0.00	0.01	0.01	0.00	0.00	0.00	0.00	0.00	0.01	0.00
Mg^{2+}	1.29	1.64	1.38	1.64	1.40	0.66	1.32	1.61	1.80	1.65	1.76	1.50	0.99	1.65
Zn^{2+}	0.00	0.00	0.00	0.00	0.00	0.00	0.00	0.00	0.00	0.00	0.00	0.00	0.00	0.00
Ni^{2+}	0.00	0.00	0.00	0.00	0.00	0.00	0.00	0.00	0.00	0.00	0.00	0.01	0.00	0.00
Vac.	0.09	0.11	0.10	0.10	0.13	0.16	0.08	0.08	0.01	0.11	0.03	0.09	0.14	0.07
Y-sum.	2.91	2.89	2.90	2.90	2.87	2.84	2.92	2.92	2.99	2.89	2.97	2.91	2.86	2.93
Ca^{2+}	0.06	0.12	0.09	0.17	0.13	0.03	0.07	0.04	0.00	0.07	0.01	0.05	0.04	0.06
Na^{+}	0.75	0.71	0.80	0.66	0.60	0.60	0.78	0.51	0.92	0.81	0.90	0.71	0.56	0.78
K^{+}	0.00	0.00	0.00	0.00	0.00	0.01	0.00	0.00	0.01	0.00	0.01	0.00	0.01	0.00
Vac.	0.19	0.17	0.11	0.17	0.27	0.36	0.15	0.45	0.07	0.11	0.08	0.23	0.39	0.15
X-sum.	0.81	0.83	0.89	0.83	0.73	0.64	0.85	0.55	0.93	0.89	0.92	0.77	0.61	0.85
F^{-}	0.00	0.00	0.00	0.00	0.00	0.00	0.00	0.00	0.00	0.00	0.00	0.00	0.00	0.00
Cl^{-}	0.00	0.00	0.00	0.00	0.00	0.00	0.00	0.00	0.00	0.00	0.00	0.00	0.01	0.00
OH^{-}	3.71	3.65	3.67	3.67	3.58	3.46	3.73	3.73	4.00	3.72	4.00	3.71	3.53	3.88
O^{2-}	0.29	0.35	0.33	0.33	0.42	0.54	0.27	0.27	0.00	0.28	0.00	0.29	0.46	0.11
$V+W_{sum.}$	4.00	4.00	4.00	4.00	4.00	4.00	4.00	4.00	4.00	4.00	4.00	4.00	4.00	4.00
$Cat._{sum.}$	18.72	18.73	18.79	18.73	18.60	18.48	18.76	18.47	18.93	18.80	18.92	18.68	18.47	18.81
Al_{sum}	6.21	6.18	6.06	6.02	6.30	6.69	6.10	6.57	5.82	5.97	5.56	6.29	6.80	6.01

Table S2 (continued):

Formation		**JPF**								**MB**		**JPF**			
Sample	**PU-5**	**SZTOL-1**								**LIT-1**		**H-15**			
Analysis	**Tur#15**	**Tur#16**	**Tur#17**	**Tur#18**	**Tur#19**	**Tur#20**	**Tur#21**	**Tur#22**	**Tur#23**	**Tur#24**	**Tur#25**	**Tur#26**	**Tur#27**	**Tur#28**	**Tur#29**
SiO_2	36.51	36.49	36.24	37.00	35.21	36.91	36.66	36.19	36.05	35.05	34.82	36.73	37.51	36.73	37.29
TiO_2	1.05	0.85	1.34	0.48	0.78	1.18	0.59	0.76	0.69	1.08	1.14	0.78	0.86	1.02	0.60
B_2O_3*	10.51	10.54	10.53	10.76	10.50	10.75	10.53	10.47	10.42	10.41	10.22	10.81	10.82	10.83	10.90
Al_2O_3	30.14	30.56	30.20	33.18	33.33	31.49	28.21	27.10	28.48	32.15	30.46	32.90	31.37	33.01	33.20
Cr_2O_3	0.16	0.04	0.00	0.02	0.00	0.14	0.00	0.01	0.01	0.05	0.03	0.00	0.09	0.09	0.02
V_2O_3	0.00	0.00	0.00	0.00	0.00	0.00	0.00	0.00	0.00	0.00	0.00	0.00	0.00	0.00	0.00
Fe_2O_3*	0.00	0.00	0.00	0.00	0.00	0.00	2.44	4.56	1.81	0.00	0.00	0.00	0.00	0.00	0.00
FeO	10.56	10.23	11.18	9.18	13.29	7.53	9.08	8.76	12.27	8.01	8.45	5.53	5.49	5.72	5.83
MnO	0.01	0.01	0.03	0.01	0.10	0.01	0.00	0.00	0.05	0.07	0.03	0.00	0.00	0.00	0.00
MgO	5.60	5.88	5.48	5.59	2.64	7.22	7.44	7.33	5.43	5.78	6.13	7.93	8.80	7.68	7.69
NiO	0.05	0.00	0.00	0.02	0.01	0.00	0.00	0.00	0.03	0.01	0.02	0.00	0.00	0.00	0.00
ZnO	0.00	0.00	0.00	0.00	0.00	0.00	0.00	0.00	0.00	0.00	0.00	0.00	0.00	0.00	0.00
CaO	0.30	0.32	0.46	0.15	0.48	1.01	0.06	0.05	0.06	0.81	0.35	0.85	0.41	0.95	0.75
Na_2O	2.66	2.62	2.57	2.13	1.91	2.04	2.90	2.78	2.90	1.90	2.32	2.24	2.58	2.01	2.28
K_2O	0.02	0.02	0.02	0.02	0.03	0.02	0.06	0.07	0.06	0.03	0.01	0.04	0.03	0.04	0.03
H_2O*	3.35	3.42	3.40	3.54	3.42	3.35	3.63	3.61	3.59	3.27	3.34	3.37	3.49	3.35	3.36
F	0.00	0.00	0.00	0.00	0.00	0.00	0.00	0.00	0.00	0.00	0.00	0.00	0.00	0.00	0.00
Cl	0.00	0.00	0.00	0.00	0.00	0.00	0.00	0.00	0.00	0.00	0.00	0.01	0.00	0.00	0.00
Total	100.93	100.97	101.46	102.10	101.70	101.66	101.61	101.70	101.84	98.63	97.33	101.20	101.45	101.45	101.96
Si^{4+}	6.04	6.02	5.98	5.98	5.83	5.97	6.05	6.01	6.01	5.85	5.92	5.91	6.02	5.89	5.95
Al^{3+}	0.00	0.00	0.02	0.02	0.17	0.03	0.00	0.00	0.00	0.15	0.08	0.09	0.00	0.11	0.05
T-sum.	6.04	6.02	6.00	6.00	6.00	6.00	6.05	6.01	6.01	6.00	6.00	6.00	6.02	6.00	6.00
B^{3+}	3.00	3.00	3.00	3.00	3.00	3.00	3.00	3.00	3.00	3.00	3.00	3.00	3.00	3.00	3.00
Al^{3+}	5.87	5.94	5.86	5.97	5.92	5.81	5.49	5.30	5.60	5.85	5.93	5.85	5.92	5.82	5.87
Cr^{3+}	0.02	0.01	0.00	0.00	0.00	0.02	0.00	0.00	0.00	0.01	0.00	0.00	0.01	0.01	0.00
V^{3+}	0.00	0.00	0.00	0.00	0.00	0.00	0.00	0.00	0.00	0.00	0.00	0.00	0.00	0.00	0.00
Mg^{2+}	0.05	0.06	0.08	0.03	0.08	0.18	0.01	0.01	0.01	0.14	0.06	0.15	0.07	0.16	0.13
Fe^{3+}	0.05	0.00	0.06	0.00	0.00	0.00	0.50	0.69	0.39	0.00	0.00	0.00	0.00	0.00	0.00
Z-sum.	6.00	6.00	6.00	6.00	6.00	6.00	6.00	6.00	6.00	6.00	6.00	6.00	6.00	6.00	6.00
Ti^{4+}	0.13	0.11	0.17	0.06	0.10	0.14	0.07	0.09	0.09	0.14	0.15	0.09	0.10	0.12	0.07
Al^{3+}	0.00	0.00	0.00	0.32	0.41	0.16	0.00	0.00	0.00	0.33	0.09	0.29	0.02	0.31	0.32
Fe^{3+}	0.00	0.00	0.00	0.00	0.00	0.00	0.00	0.00	0.00	0.00	0.00	0.00	0.00	0.00	0.00
Fe^{2+}	1.41	1.41	1.48	1.24	1.84	1.02	1.06	1.10	1.55	1.12	1.20	0.74	0.74	0.77	0.78
Mn^{2+}	0.00	0.00	0.00	0.00	0.01	0.00	0.00	0.00	0.01	0.01	0.00	0.00	0.00	0.00	0.00
Mg^{2+}	1.33	1.39	1.27	1.32	0.57	1.56	1.82	1.80	1.34	1.30	1.49	1.76	2.04	1.67	1.70
Zn^{2+}	0.00	0.00	0.00	0.00	0.00	0.00	0.00	0.00	0.00	0.00	0.00	0.00	0.00	0.00	0.00
Ni^{2+}	0.01	0.00	0.00	0.00	0.00	0.00	0.00	0.00	0.00	0.00	0.00	0.00	0.00	0.00	0.00
Vac.	0.13	0.09	0.08	0.06	0.07	0.12	0.05	0.01	0.01	0.11	0.07	0.12	0.10	0.12	0.13
Y-sum.	2.87	2.91	2.92	2.94	2.93	2.88	2.95	2.99	2.99	2.89	2.93	2.88	2.90	2.88	2.87
Ca^{2+}	0.05	0.06	0.08	0.03	0.08	0.18	0.01	0.01	0.01	0.14	0.06	0.15	0.07	0.16	0.13
Na^{+}	0.85	0.84	0.82	0.67	0.61	0.64	0.93	0.89	0.94	0.62	0.77	0.70	0.80	0.63	0.71
K^{+}	0.00	0.00	0.00	0.00	0.01	0.00	0.01	0.01	0.01	0.01	0.00	0.01	0.01	0.01	0.01
Vac.	0.09	0.10	0.09	0.30	0.30	0.18	0.05	0.08	0.04	0.23	0.17	0.15	0.12	0.20	0.16
X-sum.	0.91	0.90	0.91	0.70	0.70	0.82	0.95	0.92	0.96	0.77	0.83	0.85	0.88	0.80	0.84
F^{-}	0.00	0.00	0.00	0.00	0.00	0.00	0.00	0.00	0.00	0.00	0.00	0.00	0.00	0.00	0.00
Cl^{-}	0.00	0.00	0.00	0.00	0.00	0.00	0.00	0.00	0.00	0.00	0.00	0.00	0.00	0.00	0.00
OH^{-}	3.69	3.76	3.74	3.82	3.77	3.62	4.00	4.00	4.00	3.64	3.78	3.61	3.74	3.59	3.58
O^{2-}	0.31	0.24	0.26	0.18	0.23	0.38	0.00	0.00	0.00	0.36	0.22	0.39	0.26	0.41	0.42
$V+W_{sum.}$	4.00	4.00	4.00	4.00	4.00	4.00	4.00	4.00	4.00	4.00	4.00	4.00	4.00	4.00	4.00
$Cat._{sum.}$	18.82	18.83	18.83	18.64	18.63	18.70	18.95	18.92	18.96	18.66	18.77	18.73	18.80	18.67	18.71
$Al_{sum.}$	5.87	5.94	5.87	6.32	6.50	6.00	5.49	5.30	5.60	6.33	6.10	6.24	5.94	6.24	6.24

Table S2 (continued):

Formation	MB				JPF						JPF					
Sample	MIL-2				DRAB-3						KRC-5					
Analysis	Tur#30	Tur#31	Tur#32	Tur#43	Tur#43	Tur#43	Tur#36	Tur#37	Tur#38	Tur#39	Tur#40	Tur#41	Tur#42	Tur#43	Tur#44	Tur#45
SiO_2	37.40	36.16	34.71	36.32	36.32	36.32	36.80	37.44	37.19	36.86	36.39	35.65	35.76	36.32	35.81	35.84
TiO_2	0.24	0.30	4.37	0.82	0.82	0.82	0.75	1.07	0.27	1.36	0.79	0.86	0.68	0.82	0.46	0.12
B_2O_3*	10.88	10.53	10.27	10.68	10.68	10.68	10.69	10.79	10.93	10.63	10.51	10.65	10.56	10.68	10.48	10.31
Al_2O_3	34.16	31.21	26.50	33.71	33.71	33.71	31.69	31.53	35.07	30.29	29.18	33.98	33.74	33.71	33.31	27.55
Cr_2O_3	0.05	0.03	0.02	0.11	0.11	0.11	0.03	0.04	0.03	0.04	0.00	0.12	0.03	0.11	0.01	0.04
V_2O_3	0.00	0.00	0.00	0.00	0.00	0.00	0.00	0.00	0.00	0.00	0.00	0.00	0.00	0.00	0.00	0.00
Fe_2O_3*	0.00	0.00	0.00	0.00	0.00	0.00	0.00	0.00	0.00	0.00	1.42	0.00	0.00	0.00	0.00	2.91
FeO	5.95	9.41	11.97	5.92	5.92	5.92	7.15	7.60	5.87	8.01	6.88	5.51	9.33	5.92	11.24	8.41
MnO	0.01	0.06	0.09	0.00	0.00	0.00	0.03	0.02	0.05	0.05	0.04	0.00	0.06	0.00	0.06	0.01
MgO	7.13	6.50	5.71	6.47	6.47	6.47	7.39	7.16	6.56	7.31	8.34	6.70	4.44	6.47	3.24	7.61
NiO	0.00	0.00	0.01	0.00	0.00	0.00	0.02	0.00	0.01	0.01	0.00	0.00	0.04	0.00	0.01	0.00
ZnO	0.00	0.00	0.00	0.00	0.00	0.00	0.00	0.00	0.00	0.00	0.00	0.00	0.00	0.00	0.00	0.00
CaO	0.28	0.18	1.00	0.20	0.20	0.20	0.64	0.20	0.50	0.54	0.00	1.03	0.54	0.20	0.79	0.41
Na_2O	1.89	2.75	2.24	2.24	2.24	2.24	2.21	2.59	2.00	2.28	2.76	1.62	1.57	2.24	1.36	2.71
K_2O	0.01	0.01	0.08	0.02	0.02	0.02	0.01	0.02	0.03	0.02	0.04	0.03	0.03	0.02	0.02	0.04
H_2O*	3.55	3.59	3.16	3.27	3.27	3.27	3.46	3.42	3.36	3.44	3.62	3.25	3.36	3.27	3.26	3.56
F	0.00	0.00	0.00	0.00	0.00	0.00	0.00	0.00	0.00	0.00	0.00	0.00	0.00	0.00	0.00	0.00
Cl	0.00	0.00	0.00	0.00	0.00	0.00	0.00	0.00	0.00	0.00	0.01	0.01	0.00	0.00	0.02	0.00
Total	101.56	100.72	100.13	99.76	99.76	99.76	100.86	101.89	101.86	100.83	99.98	99.42	100.13	99.76	100.07	99.52
Si^{4+}	5.97	5.97	5.87	5.91	5.91	5.91	5.98	6.03	5.92	6.03	6.02	5.82	5.89	5.91	5.94	6.04
Al^{3+}	0.03	0.03	0.13	0.09	0.09	0.09	0.02	0.00	0.08	0.00	0.00	0.18	0.11	0.09	0.06	0.00
T-sum.	6.00	6.00	6.00	6.00	6.00	6.00	6.00	6.03	6.00	6.03	6.02	6.00	6.00	6.00	6.00	6.04
B^{3+}	3.00	3.00	3.00	3.00	3.00	3.00	3.00	3.00	3.00	3.00	3.00	3.00	3.00	3.00	3.00	3.00
Al^{3+}	5.95	5.96	5.16	5.95	5.95	5.95	5.89	5.96	5.91	5.84	5.69	5.80	5.90	5.95	5.86	5.47
Cr^{3+}	0.01	0.00	0.00	0.01	0.01	0.01	0.00	0.01	0.00	0.01	0.00	0.02	0.00	0.01	0.00	0.01
V^{3+}	0.00	0.00	0.00	0.00	0.00	0.00	0.00	0.00	0.00	0.00	0.00	0.00	0.00	0.00	0.00	0.00
Mg^{2+}	0.05	0.03	0.18	0.03	0.03	0.03	0.11	0.03	0.08	0.09	0.00	0.18	0.10	0.03	0.14	0.07
Fe^{3+}	0.00	0.00	0.66	0.00	0.00	0.00	0.00	0.00	0.00	0.06	0.31	0.00	0.00	0.00	0.00	0.45
Z-sum.	6.00	6.00	6.00	6.00	6.00	6.00	6.00	6.00	6.00	6.00	6.00	6.00	6.00	6.00	6.00	6.00
Ti^{4+}	0.03	0.04	0.56	0.10	0.10	0.10	0.09	0.13	0.03	0.17	0.10	0.11	0.08	0.10	0.06	0.01
Al^{3+}	0.46	0.07	0.00	0.42	0.42	0.42	0.17	0.03	0.58	0.00	0.00	0.55	0.53	0.42	0.60	0.00
Fe^{3+}	0.00	0.00	0.00	0.00	0.00	0.00	0.00	0.00	0.00	0.00	0.00	0.00	0.00	0.00	0.00	0.00
Fe^{2+}	0.79	1.30	1.04	0.81	0.81	0.81	0.97	1.02	0.78	1.03	0.82	0.75	1.28	0.81	1.56	1.11
Mn^{2+}	0.00	0.01	0.01	0.00	0.00	0.00	0.00	0.00	0.01	0.01	0.01	0.00	0.01	0.00	0.01	0.00
Mg^{2+}	1.65	1.57	1.26	1.53	1.53	1.53	1.68	1.69	1.47	1.69	2.06	1.45	0.99	1.53	0.66	1.84
Zn^{2+}	0.00	0.00	0.00	0.00	0.00	0.00	0.00	0.00	0.00	0.00	0.00	0.00	0.00	0.00	0.00	0.00
Ni^{2+}	0.00	0.00	0.00	0.00	0.00	0.00	0.00	0.00	0.00	0.00	0.00	0.00	0.01	0.00	0.00	0.00
Vac.	0.07	0.01	0.13	0.14	0.14	0.14	0.08	0.13	0.13	0.10	0.02	0.14	0.09	0.14	0.12	0.04
Y-sum.	2.93	2.99	2.87	2.86	2.86	2.86	2.92	2.87	2.87	2.90	2.98	2.86	2.91	2.86	2.88	2.96
Ca^{2+}	0.05	0.03	0.18	0.03	0.03	0.03	0.11	0.03	0.08	0.09	0.00	0.18	0.10	0.03	0.14	0.07
Na^{+}	0.59	0.88	0.73	0.71	0.71	0.71	0.70	0.81	0.62	0.72	0.88	0.51	0.50	0.71	0.44	0.89
K^{+}	0.00	0.00	0.02	0.00	0.00	0.00	0.00	0.00	0.01	0.00	0.01	0.01	0.01	0.00	0.00	0.01
Vac.	0.36	0.09	0.07	0.26	0.26	0.26	0.19	0.15	0.29	0.18	0.11	0.30	0.40	0.26	0.42	0.03
X-sum.	0.64	0.91	0.93	0.74	0.74	0.74	0.81	0.85	0.71	0.82	0.89	0.70	0.60	0.74	0.58	0.97
F^{-}	0.00	0.00	0.00	0.00	0.00	0.00	0.00	0.00	0.00	0.00	0.00	0.00	0.00	0.00	0.00	0.00
Cl^{-}	0.00	0.00	0.00	0.00	0.00	0.00	0.00	0.00	0.00	0.00	0.00	0.00	0.00	0.00	0.00	0.00
OH^{-}	3.79	3.95	3.57	3.55	3.55	3.55	3.75	3.67	3.57	3.75	4.00	3.54	3.69	3.55	3.61	4.00
O^{2-}	0.21	0.05	0.43	0.45	0.45	0.45	0.25	0.33	0.43	0.25	0.00	0.46	0.31	0.45	0.39	0.00
$V+W_{sum.}$	4.00	4.00	4.00	4.00	4.00	4.00	4.00	4.00	4.00	4.00	4.00	4.00	4.00	4.00	4.00	4.00
$Cat._{sum.}$	18.57	18.90	18.80	18.61	18.61	18.61	18.73	18.75	18.57	18.75	18.89	18.56	18.51	18.61	18.47	18.97
Al_{sum}	6.43	6.07	5.29	6.46	6.46	6.46	6.07	5.99	6.57	5.84	5.69	6.54	6.54	6.46	6.51	5.47

Table S3: Microprobe analyses of detrital garnets from the sediments studied.

Formation	**JPF**									**JPF**		
Sample	**PU-5**									**SZTOL-1**		
Analysis	**Grt#1**	**Grt#2**	**Grt#3**	**Grt#4**	**Grt#5**	**Grt#6**	**Grt#7**	**Grt#8**	**Grt#9**	**Grt#10**	**Grt#11**	**Grt#12**
SiO_2	35.80	36.71	36.89	36.82	37.22	37.31	37.16	37.17	37.53	36.75	37.26	37.31
TiO_2	0.08	0.12	0.05	0.10	0.14	0.09	0.07	0.13	0.07	0.11	0.13	0.09
Al_2O_3	20.93	21.01	21.17	21.01	21.07	21.41	21.10	21.01	21.43	21.33	21.33	21.56
FeO	29.21	29.17	37.00	35.37	28.50	25.53	27.70	26.09	33.30	34.19	31.81	32.60
MnO	10.71	8.80	2.23	2.20	3.25	11.65	9.12	6.68	0.28	5.64	6.74	4.10
MgO	1.62	1.07	1.62	1.58	0.77	2.16	0.93	0.81	1.57	1.02	1.01	1.20
CaO	1.73	3.78	2.06	3.10	9.60	3.06	3.92	8.45	6.68	2.92	3.89	5.20
Cr_2O_3	0.07	0.02	0.00	0.00	0.01	0.06	0.02	0.01	0.03	0.04	0.02	0.02
Total	100.14	100.67	101.01	100.19	100.55	101.27	100.02	100.35	100.89	101.99	102.20	102.08
	Formula normalization to 12 oxydes and 8 cations											
Si	2.926	2.969	2.975	2.984	2.976	2.977	3.001	2.983	2.987	2.949	2.970	2.964
Al^{IV}	0.074	0.031	0.025	0.016	0.024	0.023	0.000	0.017	0.013	0.051	0.030	0.036
Al^{VI}	1.946	1.973	1.989	1.991	1.964	1.990	2.014	1.971	1.999	1.967	1.975	1.984
Ti	0.005	0.007	0.003	0.006	0.008	0.006	0.004	0.008	0.004	0.006	0.008	0.006
Cr	0.004	0.001	0.000	0.000	0.001	0.004	0.001	0.001	0.002	0.002	0.001	0.001
Fe^{3+}	0.040	0.016	0.007	0.003	0.024	0.000	0.000	0.018	0.000	0.021	0.014	0.008
Fe^{2+}	1.956	1.957	2.488	2.395	1.882	1.703	1.898	1.733	2.223	2.273	2.107	2.158
Mn	0.742	0.603	0.152	0.151	0.220	0.787	0.624	0.454	0.019	0.383	0.455	0.276
Mg	0.198	0.129	0.194	0.191	0.091	0.257	0.112	0.096	0.187	0.122	0.121	0.142
Ca	0.152	0.327	0.178	0.270	0.822	0.262	0.340	0.726	0.569	0.251	0.333	0.442
	Grt end members (mol. %)											
almandine	62.7	64.3	82.4	79.5	61.9	56.1	63.8	57.2	74.1	74.4	69.4	71.0
pyrope	6.8	4.3	6.5	6.4	3.1	8.6	3.8	3.2	6.2	4.1	4.1	4.8
grossular	2.9	10.2	5.6	8.9	26.4	8.6	11.4	23.4	19.0	7.3	10.4	14.4
spessartine	25.4	20.3	5.1	5.1	7.4	26.4	21.0	15.2	0.6	13.0	15.3	9.3
uvarovite	0.2	0.1	0.0	0.0	0.0	0.2	0.1	0.0	0.1	0.1	0.1	0.1
andradite	2.1	0.8	0.4	0.1	1.2	0.0	0.0	0.9	0.0	1.1	0.7	0.4

Table S3 (continued):

Formation	**JPF**			**MB**			**JPF**			**MB**	
Sample	**SZTOL-1**			**LIT-1**			**H-15**			**MIL-2**	
Analysis	**Grt#13**	**Grt#14**	**Grt#15**	**Grt#16**	**Grt#17**	**Grt#18**	**Grt#19**	**Grt#20**	**Grt#21**	**Grt#22**	**Grt#23**
SiO_2	37.38	37.01	37.24	36.07	34.52	35.11	36.98	37.45	37.10	36.43	36.88
TiO_2	0.03	0.05	0.09	0.00	0.05	0.07	0.07	0.08	0.03	0.05	0.05
Al_2O_3	21.35	21.43	21.44	21.22	20.66	20.89	21.12	21.25	21.53	21.22	21.52
FeO	35.80	31.80	27.41	32.65	22.54	33.79	34.18	35.56	32.45	35.36	34.87
MnO	1.55	5.47	8.15	6.21	20.49	3.80	4.56	4.20	6.19	3.87	2.94
MgO	2.57	0.84	0.67	3.01	0.56	3.23	1.31	1.49	3.28	1.48	1.40
CaO	2.98	5.21	7.08	1.09	0.45	1.54	3.62	2.32	1.28	1.96	3.14
Cr_2O_3	0.00	0.03	0.04	0.00	0.00	0.08	0.00	0.00	0.03	0.00	0.01
Total	101.67	101.84	102.12	100.25	99.28	98.51	101.84	102.33	101.88	100.36	100.82
	Formula normalization to 12 oxydes and 8 cations										
Si	2.971	2.957	2.957	2.922	2.886	2.893	2.960	2.983	2.945	2.961	2.966
Al^{IV}	0.029	0.043	0.043	0.078	0.114	0.107	0.040	0.017	0.055	0.039	0.034
Al^{VI}	1.973	1.977	1.966	1.952	1.927	1.926	1.956	1.979	1.962	1.995	2.009
Ti	0.002	0.003	0.006	0.000	0.003	0.004	0.004	0.004	0.002	0.003	0.003
Cr	0.000	0.002	0.002	0.000	0.000	0.005	0.000	0.000	0.002	0.000	0.001
Fe^{3+}	0.022	0.016	0.024	0.043	0.062	0.057	0.035	0.015	0.031	0.002	0.000
Fe^{2+}	2.358	2.109	1.797	2.169	1.514	2.271	2.253	2.353	2.123	2.402	2.362
Mn	0.105	0.370	0.548	0.426	1.451	0.265	0.309	0.283	0.416	0.266	0.200
Mg	0.305	0.100	0.079	0.364	0.070	0.397	0.156	0.176	0.388	0.179	0.168
Ca	0.254	0.446	0.602	0.094	0.040	0.136	0.310	0.198	0.108	0.171	0.271
	Grt end members (mol. %)										
almandine	77.7	69.0	58.4	69.8	45.9	72.4	73.8	78.0	69.0	79.2	78.5
pyrope	10.3	3.4	2.7	12.5	2.4	13.7	5.3	5.9	13.2	6.1	5.7
grossular	7.4	14.2	19.0	1.0	0.0	1.5	8.7	5.9	2.0	5.7	9.1
spessartine	3.5	12.5	18.5	14.6	50.3	9.2	10.4	9.5	14.1	9.0	6.8
uvarovite	0.0	0.1	0.1	0.0	0.0	0.3	0.0	0.0	0.1	0.0	0.0
andradite	1.1	0.8	1.2	2.2	1.4	3.0	1.8	0.8	1.6	0.1	0.0

Table S3 (continued):

Formation Sample	JPF KRC-5					JPF BEN-5						
Analysis	**Grt#24**	**Grt#25**	**Grt#26**	**Grt#27**	**Grt#28**	**Grt#29**	**Grt#30**	**Grt#31**	**Grt#32**	**Grt#33**	**Grt#34**	**Grt#35**
SiO_2	37.46	36.81	38.69	37.21	37.91	39.36	37.86	40.02	39.17	37.17	37.56	37.92
TiO_2	0.15	0.00	0.06	0.00	0.00	0.05	0.08	0.03	0.09	0.31	0.06	0.01
Al_2O_3	21.49	21.44	22.56	21.66	21.90	22.47	21.38	23.05	22.44	20.72	21.45	21.86
FeO	25.43	33.27	27.15	33.94	30.87	21.30	26.41	20.61	23.25	17.72	21.99	33.53
MnO	3.62	2.82	0.50	2.37	1.45	0.47	0.57	0.48	0.84	16.33	10.91	1.38
MgO	3.31	3.98	10.17	4.34	6.76	8.03	6.23	9.89	6.64	0.93	1.51	5.48
CaO	8.61	1.27	1.30	1.43	1.54	9.22	7.49	7.27	8.96	8.26	7.07	1.38
Cr_2O_3	0.01	0.02	0.02	0.00	0.02	0.00	0.04	0.01	0.00	0.05	0.03	0.00
Total	100.08	99.61	100.44	100.95	100.45	100.90	100.05	101.36	101.38	101.48	100.58	101.56
	Formula normalization to 12 oxydes and 8 cations											
Si	2.961	2.963	2.955	2.953	2.965	2.977	2.950	2.980	2.978	2.958	2.989	2.965
Al^{IV}	0.039	0.037	0.045	0.047	0.035	0.023	0.050	0.020	0.022	0.042	0.011	0.035
Al^{VI}	1.965	1.998	1.987	1.980	1.986	1.981	1.920	2.005	1.990	1.907	2.003	1.981
Ti	0.009	0.000	0.003	0.000	0.000	0.003	0.004	0.002	0.005	0.018	0.004	0.000
Cr	0.000	0.001	0.001	0.000	0.001	0.000	0.003	0.000	0.000	0.003	0.002	0.000
Fe^{3+}	0.022	0.001	0.008	0.018	0.012	0.014	0.065	0.000	0.005	0.064	0.000	0.016
Fe^{2+}	1.659	2.239	1.727	2.235	2.007	1.332	1.656	1.292	1.473	1.116	1.476	2.177
Mn	0.243	0.192	0.032	0.159	0.096	0.030	0.038	0.030	0.054	1.101	0.735	0.092
Mg	0.391	0.478	1.158	0.514	0.788	0.905	0.723	1.098	0.752	0.111	0.179	0.638
Ca	0.729	0.110	0.106	0.122	0.129	0.747	0.626	0.580	0.730	0.704	0.603	0.116
	Grt end members (mol. %)											
almandine	54.0	73.7	56.1	73.1	65.8	43.5	53.0	42.7	48.4	35.2	49.2	71.5
pyrope	13.2	16.1	39.2	17.4	26.6	30.4	24.5	36.9	25.3	3.7	6.0	21.5
grossular	23.5	3.6	3.2	3.2	3.7	24.4	17.8	19.4	24.3	20.4	20.1	3.1
spessartine	8.2	6.5	1.1	5.4	3.2	1.0	1.3	1.0	1.8	37.2	24.6	3.1
uvarovite	0.0	0.1	0.0	0.0	0.1	0.0	0.1	0.0	0.0	0.2	0.1	0.0
andradite	1.1	0.0	0.4	0.9	0.6	0.7	3.3	0.0	0.2	3.2	0.0	0.8

Table S4: Microprobe analyses of detrital spinels from the sediments studied. $*Fe_2O_3$ calculated from stoichiometry. Cr#=Cr/(Cr+Al); $Mg\#=Mg/(Mg+Fe^{2+})$. Criteria for alteration degrees according to Mikuš &Spišiak (2007); U — unaltered fresh spinel.

Formation Sample	JPF PU-5		JPF Sztol-1	MB LIT-1		JPF H-15			JPF DRAB-3	JPF KRC-5				
Analysis **Degree of alteration**	**Spl#1** **U**	**Spl#2** **U**	**Spl#3** **I**	**Spl#4** **U**	**Spl#5** **I**	**Spl#6** **I**	**Spl#7** **U**	**Spl#8** **U**	**Spl#10** **II**	**Spl#11** **U**	**Spl#12** **U**	**Spl#13** **U**	**Spl#14** **U**	**Spl#15** **U**
SiO_2	0.09	0.02	0.00	0.01	0.03	0.04	0.03	0.01	0.00	0.01	0.01	0.00	0.04	0.01
TiO_2	0.31	0.05	0.30	0.05	0.02	0.08	0.10	0.09	3.26	0.08	0.04	0.08	0.06	0.04
V_2O_5	0.12	0.24	0.23	0.12	0.31	0.04	0.16	0.07	0.36	0.25	0.22	0.21	0.22	0.19
Al_2O_3	36.62	23.97	12.76	42.58	19.95	25.20	36.39	51.65	6.83	23.73	19.84	26.47	26.57	25.73
Cr_2O_3	29.69	47.46	55.73	25.73	49.55	41.63	32.67	17.63	35.05	47.35	51.53	43.51	43.23	45.44
$Fe_2O_3^*$	5.48	2.40	4.16	1.98	1.22	5.56	3.08	2.14	23.89	1.57	1.50	2.25	1.49	1.73
FeO	13.07	12.39	21.25	12.21	17.83	18.57	14.91	10.70	28.64	15.70	15.27	15.49	12.05	12.64
MnO	0.28	0.33	0.43	0.24	0.44	0.35	0.26	0.14	0.43	0.30	0.39	0.33	0.25	0.26
MgO	16.27	15.51	8.68	16.98	11.10	11.65	15.26	19.35	2.30	13.31	13.07	13.60	15.39	15.37
CoO	0.00	0.00	0.00	0.00	0.00	0.00	0.00	0.00	0.00	0.00	0.00	0.00	0.00	0.00
NiO	0.11	0.13	0.04	0.24	0.02	0.10	0.12	0.28	0.34	0.11	0.07	0.07	0.15	0.14
ZnO	0.08	0.05	0.28	0.21	0.12	0.26	0.12	0.17	0.26	0.12	0.11	0.23	0.10	0.05
Total	101.57	102.30	103.45	100.15	100.46	102.92	102.80	102.01	98.97	102.38	101.91	102.03	99.39	101.43
	Based on 3 cations													
Cr	0.660	1.106	1.406	0.564	1.226	0.984	0.725	0.364	0.981	1.120	1.244	1.019	1.022	1.060
Ti	0.007	0.001	0.007	0.001	0.001	0.002	0.002	0.002	0.087	0.002	0.001	0.002	0.001	0.001
V	0.002	0.005	0.005	0.002	0.006	0.001	0.003	0.001	0.008	0.005	0.004	0.004	0.004	0.004
Al	1.214	0.833	0.480	1.391	0.736	0.888	1.204	1.591	0.285	0.837	0.714	0.924	0.937	0.896
Fe^{3+}	0.108	0.048	0.089	0.038	0.023	0.123	0.061	0.039	0.543	0.029	0.030	0.045	0.029	0.034
Fe^{2+}	0.315	0.310	0.578	0.286	0.472	0.466	0.355	0.237	0.942	0.399	0.395	0.389	0.306	0.316
Mn	0.007	0.008	0.012	0.006	0.012	0.009	0.006	0.003	0.013	0.008	0.010	0.008	0.006	0.007
Mg	0.682	0.682	0.413	0.701	0.518	0.519	0.638	0.754	0.121	0.593	0.595	0.600	0.686	0.676
Co	0.000	0.000	0.000	0.000	0.000	0.000	0.000	0.000	0.000	0.000	0.000	0.000	0.000	0.000
Ni	0.003	0.003	0.001	0.005	0.000	0.002	0.003	0.006	0.010	0.003	0.002	0.002	0.004	0.003
Zn	0.002	0.001	0.007	0.004	0.003	0.006	0.002	0.003	0.007	0.003	0.002	0.005	0.002	0.001
Total	2.999	2.998	2.998	2.999	2.997	3.000	2.999	2.999	2.996	2.998	2.998	2.998	2.998	2.998
Cr#	35	57	75	29	62	53	38	19	77	57	64	52	52	54
Mg#	68	69	42	71	52	53	64	76	11	60	60	61	69	68
Fe^{2+}/Fe^{3+}	2.9	6.4	6.5	7.5	20.6	3.8	5.9	6.1	1.7	13.6	13.2	8.7	10.6	9.2